Multi-Scale State of Stress Analysis of the Potiguar Basin NE Brazil

L.J. (Luc) Kroon

Multi-Scale State of Stress Analysis of the Potiguar Basin NE Brazil

by

L.J. (Luc) Kroon

to obtain the degree of Master of Science
at the Delft University of Technology,
to be defended publicly on Monday September 11, 2017 at 10:00 AM.

Student number:	4409779	
Project duration:	July 1, 2016 – September 1, 2017	
Thesis committee:	Prof. dr. G. Bertotti	TU Delft, supervisor
	Dr. A. Barnhoorn	TU Delft
	Dr. J. E. A. Storms	TU Delft

TU Delft

Contents

1

Introduction

Carbonate formations have been of large interest in the Exploration and Production (E&P) industry in recent years due to potential that lies in these reservoirs and rank among the largest hydrocarbon reserves in the world. Presence of fractures in these tight carbonate formations will increase producibility and fluid flow will be controlled by the orientation and spacing of these fractures. These fractures are created by the application of stress on the brittle carbonate formations and are often basin wide. Better knowledge of the paleo-stress fields involved in the fracturing of the formations and the correlation with the orientation, density and spacing of the fractures present in the formation (Bisdom et al., 2016) will allow for stress predictions in basins of a similar setting. This study has a multi-scale focus on the construction and constraining of the geomechanical model. Small scale outcrop studies throughout Potiguar basin and large scale geomechanical basin modelling allowed for independant analysis of the state of stress in both the small scale and large scale as well as providing better constraints for the geomechanical model. On the small scale, recent developments in stylolite analysis (Schmittbuhl et al., 2004; Ebner, 2009; Koehn et al., 2012) allows for the quantification of stresses of paleo-stress fields. Combined with the timing of the tectonic events, their principal stress orientations and stress/strain relations leads to the determination of paleo-stress fields on the small scale. On the large scale, the basin geometry, sedimentary composition and extent allow for the construction of a geological model of the basin. Implementation of the geomechanical properties of each facies then allows for geomechanical calculations. These calculations determine the distribution and orientation of principal stresses throughout the basin for various scenarios of tectonic history. By comparison with the structural data, the numerical geomechanical model can be better constrained.

In North-East Brazil, the Potiguar basin is a failed rift basin upon which the fractured carbonate Jandaira formation is exposed. The Potiguar basin encompasses both the onshore and offshore portions of the easternmost equatorial marginal basin of Brazil and covers an area of 48,000 km^2. The Potiguar basin has a long history of geological research due to the presence of hydrocarbons. Knowledge of the basin geometry and the extent of the basin formations are well documented (Bertani et al., 1987; Couto Anjos et al., 1990; Sampaio, A.V., Schaller, H., 1968; Araripe, P. de T., Feijo, F. J., 1994). In recent years, extensive research on the Potiguar basin has been done to determine the depth of the basement throughout the basin and the characteristics of the bounding faults by the Universidade Federal do Rio Grande do Norte (UFRN) (Neto et al., 2007;Reis et al., 2013; de Melo, 2016). The rift geometry is characterized by the asymmertric horst and graben structures, trending NE-SW, and the bounding faults of the Apodi fault system in the South-East of the basin, which have offsets of up to 5 kilometers (Bertani et al., 1990; Matos, 1992) (Figure 1.1).The Jandaira formation is outcropping in a near-horizontally dipping pavement with an area of 100 km x 100 km and allows for top views of the fractured formation. Despite significant karstification of the limestones, the fracture systems are still clearly visible.

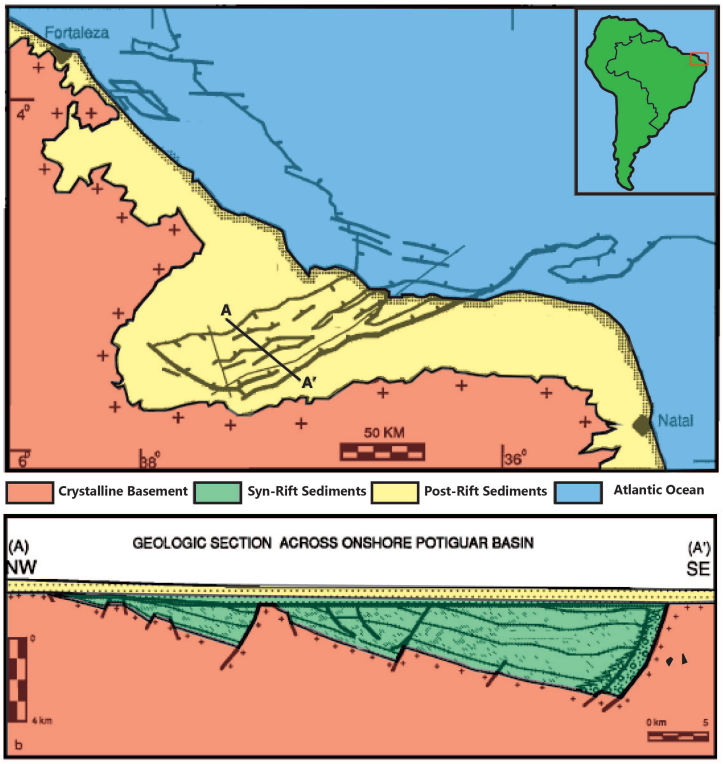

Figure 1.1: The Potiguar basin in North-East Brazil. In red is shown the crystalline basement and in yellow the Mesozoic rift sediments. The major faults are also shown, as well as a cross-section throughout the central area of the rift that shows the asymmetric geometry of the basin. The figure is modified after Matos, 1992.

The aim of this study is to construct a geomechanical basin model that represents the spatial distriubtion of the orientation of the principal stresses and the quantification of vertical and horizontal stresses present during the formation of the structural features in Jandaira formation. The study consists of outcrop examination, stylolite trace analysis and the geomechancial model. The outcrop examination and stylolite analysis have been developed separate from the geomechanical model and function to further validate and constrain the model. In the first section concerning outcrop analysis, structural features of the Jandaira outcrops determined principal stress orientations, the timing of the events and the presence of stress/strain relations. This was integrated with similar research (de Graaf, 2015;Oskam 2015;Bertotti, 2017) on outcrops at different locations in the basin. Integration of all data will provide the basin wide variations of the stress orientations and will this will be compared with the results from the geomechanical model.

The second section is concerned with stress determination from stylolite samples. Previous research based on Fourier analysis of stylolite traces (length and amplitude) is used to determine the maximum amount of stress exerted on the rock (Schmittbuhl et al., 2004; Ebner, 2009; Koehn et al., 2012). Modifications of the equations have been implemented to include horizontal (tectonic) forces and this has been examined for the Jandaira formation (Oskam, 2015;Bertotti, 2017). This study also adopted this method and further analysis was performed on different sections of the Jandaira formation to add to and constrain the results of the previous efforts.

The third section of this study concerns the geomechanical model, which is constructed using the well defined basin geometry from previous studies (Bertani et al., 1987; Couto Anjos et al., 1990; De Melo, 2016). Through further cooperation with the geoscience department of the UFRN, addditional basin geometry data was provided which was used to create a basin model with the geological modeling software and a subsequent geomechanical model. Several scenario's were considered with a base case of only uni-axial burial conditions, two scenario of compression and a scenario of the present day conditions in the Potiguar basin. Principal stress orientations and in particular the local rotation and maximum burial depth results from the previous sections were compared with the results of the geomechanical model.

2

Geological Setting

The Potiguar Basin is a mature rift basin located on the North-East of Brazil and consists of pre-rift crystalline rocks, syn-rift and post-rift sediments. The syn-rift basin is bound on the East and South by large fault systems of respectively Umbuzeiro and Apodi (Melo, 2016) and thins towards the Western section of the basin. Post-rift deposits are present throughout the onshore and offshore parts of the Potiguar basin and thin out towards the Western/Southern/Eastern sections of the basin. Basin geometry is defined by the pre-existing Neoproterozoic weak zones and extends in the NE-SW direction.

The pre-rift basement consists of crystalline rocks of the Borborema Province Precambrian shield that comprises of Archean and Proterozoic aged sections merged together during the Brasiliano orogeny of 760-540 Ma (Matos, 2000; Kirkpatrick, 2013). Shear zones and fold belts are present throughout the Borborema Province that were generated during this time period. The shear zones have an E-W trending direction and the fold belts have a NE-SW trend (Figure 2.1). Crystalline rocks of the basement are outcropping towards the

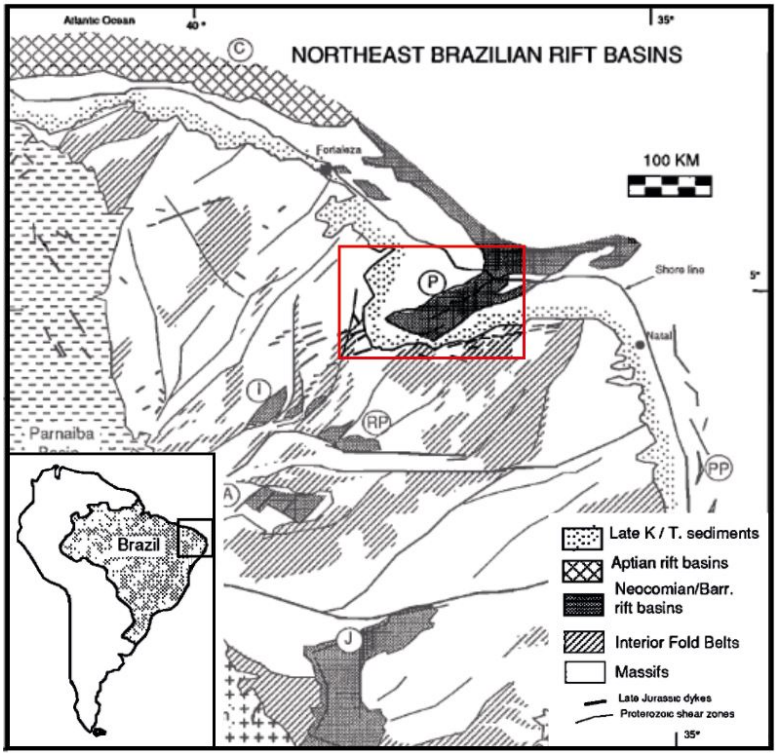

Figure 2.1: Northern Borborema Precambrian shield with the Proterozoic weak zones indicated by the shear zones and interior fold belts. The Potiguar basin is indicated in by the red box.

West and South of the Basin.

Rifting was in the basin started in the Late Jurassic/Early Neocomian and is characterized by three syn-rift phases (Matos, 1992). The first rifting phase occurred in the Late Jurassic/Early Neocomian. Late Jurassic sedimentation occurred in extensive shallow depressions and igneous dikes were formed with trends between NE-SW and E-W (figure 2.2). These indicate the onset of the break-up between the South American plate and the African plate. The second rifting phase was marked by the devolpment of major rift valleys associated with transverse megashear zones and major faulting during the Neocomian-Early Barremian age (Matos, 1992). The major faults in the East and South of the basin defined the asymmetric shape of the tilted grabens that are present throughout the base of the rift sediments. In the Early Cretaceous, the third syn-rift phase represents a major change in the rifting kinematics as the NW-SE trending extensional regime acquired an E-W orientation (Matos, 2000). Fault offsets further increased as the basin deepened and offsets of up to 5 km were developed at the Apodi and Umbuzeiro fault systems in the East section of the Potiguar basin (Melo, 2016). Sedimentation during the rifting event in the Pendencia formation is characterized by a lacustrine environment with fluvial-deltaic deposits at the fringes of the basin (Araripe and Feijo, 1994). Overlying the Pendencia formation are the transitional Pescada, Alagamar and Acu formations, deposited in fluvial setting with marine transgressions. The following Jandaira formation marks the transition to a marine environment with predominantly carbonate sediments. Figure 2.2 shows the stratigraphy in the Potiguar basin (modified from Pessoa Neto et al. (2007)).

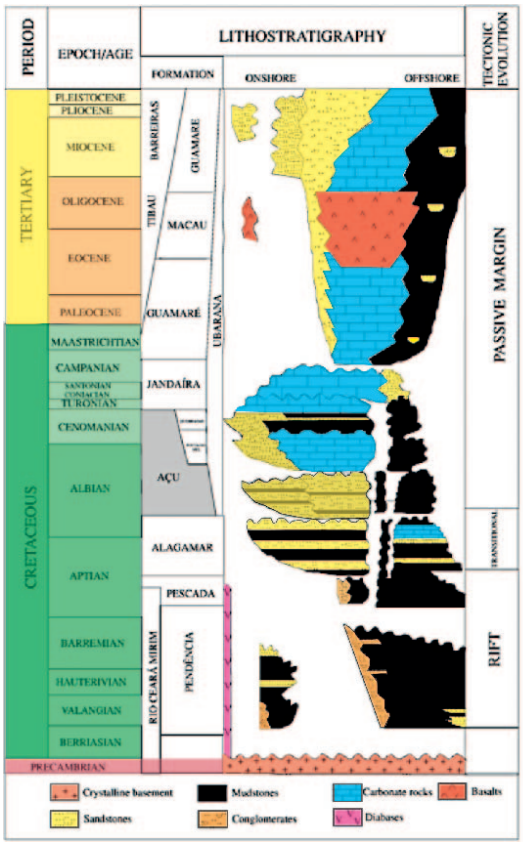

Figure 2.2: Stratigraphic column of the Potiguar basin (modified from Marachin et al. (2004)).

In the Middle Campanian a tectonic event occurred along the Atlantic margin of Brazil and caused the reactivation of the basin tectonics in the Potiguar basin. This reactivation event lead to regional uplift of the basin, resulting in an elevated position of the Jandaira formation (Gurgel et al. 2013). The post-rift sediments in the offshore section were not affected by the reactivation. Following the tectonic event, sedimentation processes ceased on the present day onshore Potiguar basin until the Miocene when the Bareiras formation was deposited. Present day stress orientations in the Potiguar basin were determined from wellbore breakouts and indicate compression of roughly E-W orientation along in the South of the basin, parallel to the continental margin and locally rotates approximately 90 degrees to a roughly N-S orientation in the Western part of the basin (Reis et al., 2013). The E-W compressional force are related to the ridge push process in the Southern Atlantic and the plate contact in the Western section of the South American plate with the Nazcan plate.

3

Section I - Outcrop analysis

In this section, the aim is to determine the regional distribution of the principal stress orientations through the examination of the structural features present at outcrops in the Potiguar basin. The UFRN has done a large amount of studies throughout the Jandaira formation and is served as a base in this study. Similar studies were also conducted in the central zone of the basin Potiguar basin (Hameka, 2013; van Eijk, 2013; de Graaf, 2014; Oskam, 2015). The areas examined in this study cover the edges of the Jandaira formation (figure 3.1) and previous results are integrated in order to determine spatial variations of the principal stress orientations throughout the basin.

3.1. Method

The study areas were examined in this study using multiple smaller stations per study area of approximately 1 x 1 m in size. For each station, the orientation, dip/dip direction, length and quality of structural features were mapped. Structural features of the Jandaira formation include open fractures, stylolites (horizontal and vertical) and veins. The quality of the structural features is an important factor as it determines the relative weight that can be applied to the resulting interpretation of the feature. The quality of the structural features is determined by several factors such as the visibility, size and density and ranges between certainty - A, and questionable - C. In this section the main structural features of each outcrop and the interpretation will be discussed. The interpretations will be combined with the previous findings to construct the regional distribution of principal stress orientations of the Jandaira formation.

Principal stress orientations were determined from the structural features in the area. σ_1 is determined from stylolites where the direction of σ_1 is perpendicular to the surface of the stylolite. σ_3 is determined from mode I fractures and constitutes the direction perpendicular to the strike of the feature or parallel to the opening direction. σ_2 is the remaining direction perpendicular to both σ_1 and σ_3 .

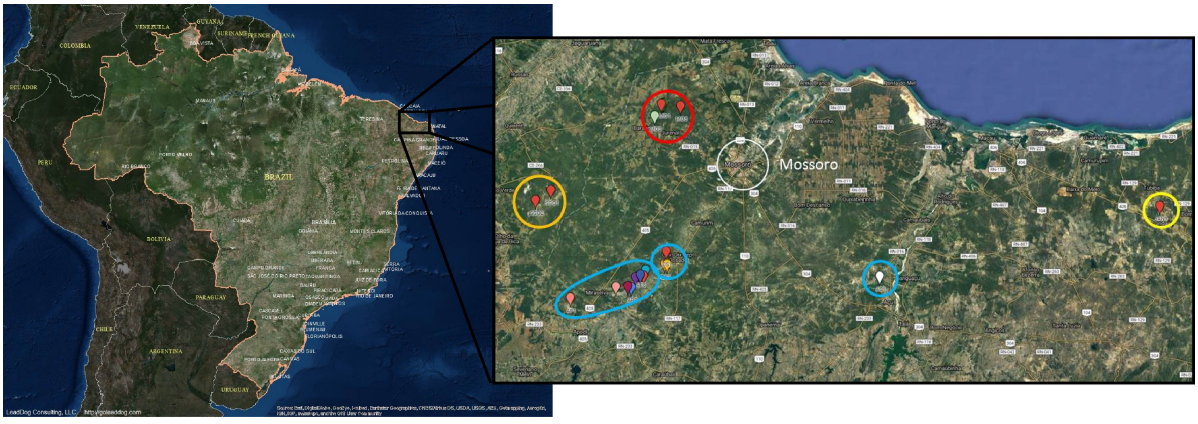

Figure 3.1: The location of the Potiguar basin in the North-East of Brazil and the position of the studied outcrops; Sao Geraldo (orange outline), Mossoro (red outline) and Jandaira (yellow outline) as well as the previously studied outcrops (blue outline).

3.2. Results

3.2.1. Sao Geraldo area

The Sao Geraldo area is located in the Western part of the Portiguar basin and consists of stations SGO 2 and SGO 3. Structural features of the outcrop are open fractures that have been subject to severe karstification, sub-horizontal stylolites and veins. Two sets of fracture systems have been observed in this outcrop; one with an orientation of 30 degrees NE and one with a dip direction of 310 degrees NW (figure 3.2a). Both fracture systems have a near vertical dip and show little to no displacement. Veins in the Sao Geraldo stations are orientated have a NW-SE strike with a vertical dip. No vertical stylolites were present in the Sao Geraldo area. Shear features are observed for the NE-SW trending fracture system (figure 3.2b) but the scarcity of these features compared to the abundance of fractures implies that this might not be very large. The absence of conjugate fractures and displacement along the fractures and indicate mode I fractures with a σ_3 perpendicular to the strike of the fracture systems. Figure 3.3 depicts the measurements taken from the Sao Geraldo outcrop in a stereoplot and rose plot. The NW-SE trending and NE-SW trending fracture systems and the NW-SE trending veins are indicative of two separate compressional episodes. One compressional episode with a horizontal σ_3 trending NW-SE and the other compressional episode has a horizontal σ_3 trending NE-SW. No structural features were present to indicate an orientation of σ_1.

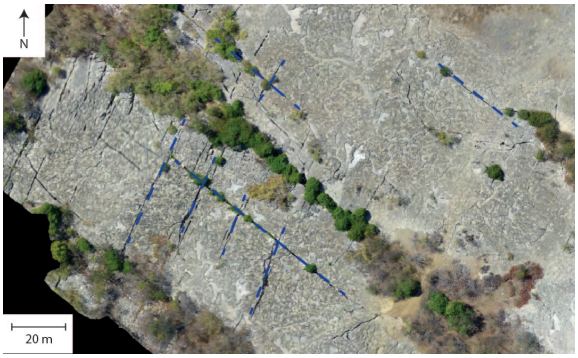

(a) Top view of the Sao Geraldo outcrop taken from a drone. Fracturing of the formation is present in two fracture systems oriented NW-SE and NE-SW (blue).

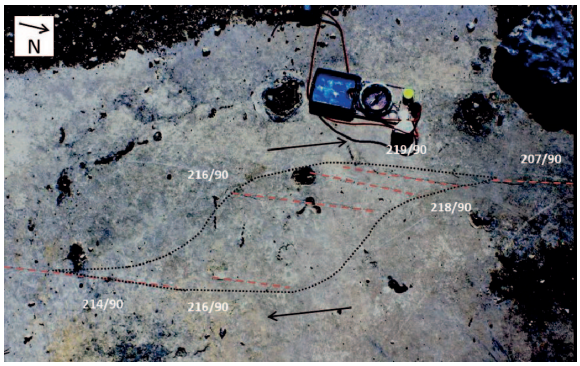

(b) Veins with shear characteristics observed on the Sao Gerald outcrop. The veins decrease in density in the middle of the shear zone and increase in density towards the end. This is indicative of dextral shear.

Figure 3.2: Structural features of the Sao Geraldo outcrop.

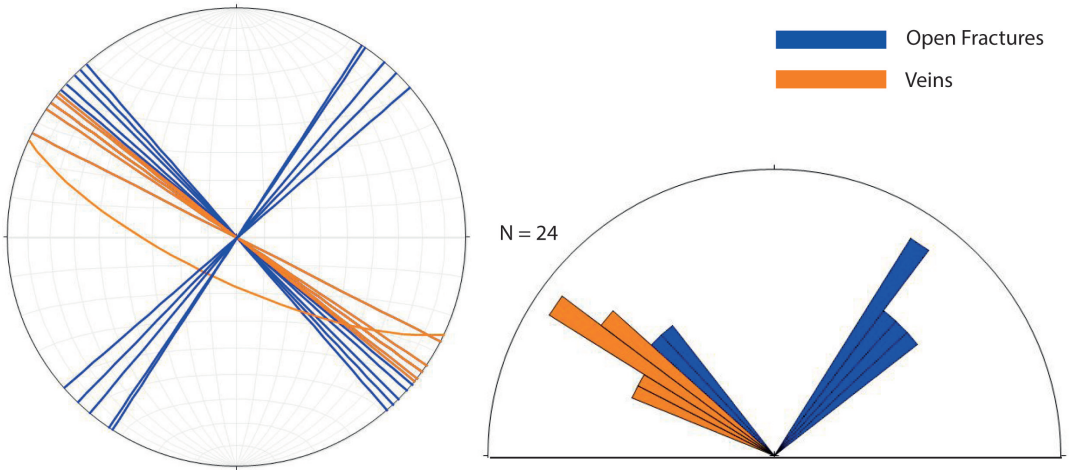

Figure 3.3: Stereoplot (left) and Rose plot (right) of the structural features of the Sao Geraldo outcrop.

3.2.2. Mossoro area

The Mossoro area is located in the Northwest of the basin and consists of stations MO 3, MO 4 and MO 5. The Mossoro area has open fractures with an orientation trending 50 degrees NE/SW with a vertical dip. Veins were observed in the outcrop with both the NE-SW and NW-SE orientations. Vertical stylolites were present in the outcrops that (figure 3.4a) with a near vertical dip of 85 degrees and a dip direction of 30 degrees NE. No shear features could be found in the Mossoro outcrop. Relative timing relations were observed in this outcrop as the abundant horizontal stylolites show displacement of the vertical stylolites and veins (figure 3.4b).

Figure 3.5 depicts the measurements taken from the Mossoro outcrop in a stereoplot and rose plot. As vertical stylolites are formed perpendicular to σ_1, indicative of a compressional NE-SW oriented σ_1. Veins of NW-SE and NE-SW orientation indicate a σ_3 of NE-SW and NW-SE orientation.

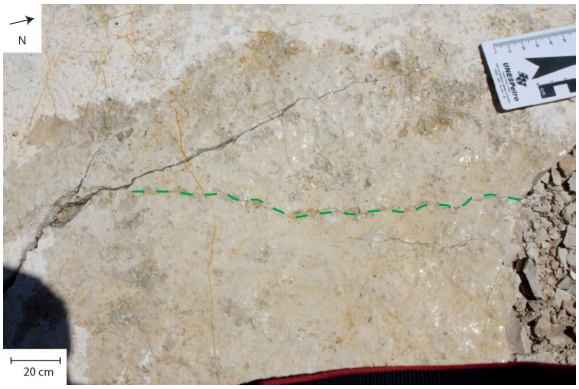

(a) Top view of a sub-vertical stylolite on the Mossoro outcrop.

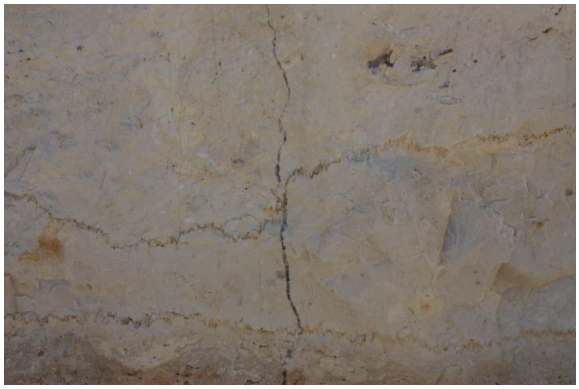

(b) Vertical vein of the Mossoro outcrop displaced by a sub-horizontal stylolite.

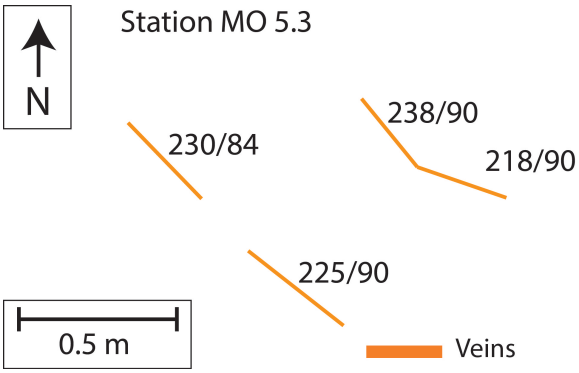

(c) Measurements of the MO 5.3 station.

Figure 3.4: Example measurement station MO5.3.

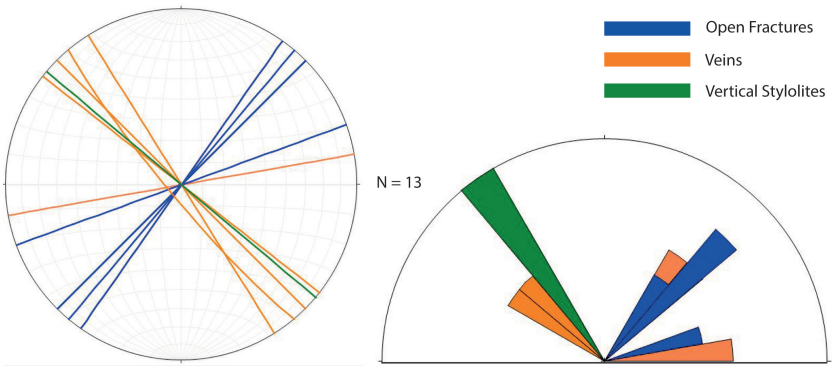

Figure 3.5: Stereoplot (left) and Rose plot (right) of the structural features of the Mossoro outcrop.

3.2.3. Jandaira area

The Jandaira outcrop is located in the East of the Portiguar basin and consist of stations Jan 1.1 through Jan 1.6. Structural features in this outcrop are limited to two sets of fracture systems trending E-W and N-S (figure 3.6a and 3.6b). No displacement nor shear indicators were clearly visible in the outcrop, leading to mode I fractures. Relative timing was not possible from fracture or abutment relations.

Figure 3.7 depicts the measurements taken from the Jandaira outcrop in a stereoplot and rose plot. Only open fractures were present in the outcrop and are indicative of multiple periods of fracturing with σ_3 oriented to the NW-SE and NE-SW, respectively.

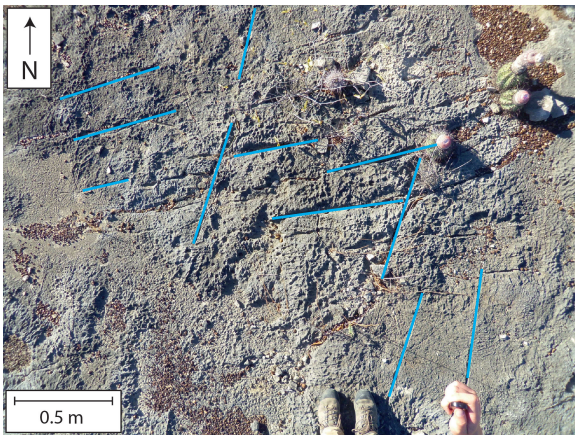

(a) Mode I fractures of predominantly E-W (red) and N-S (yellow) azimuth.

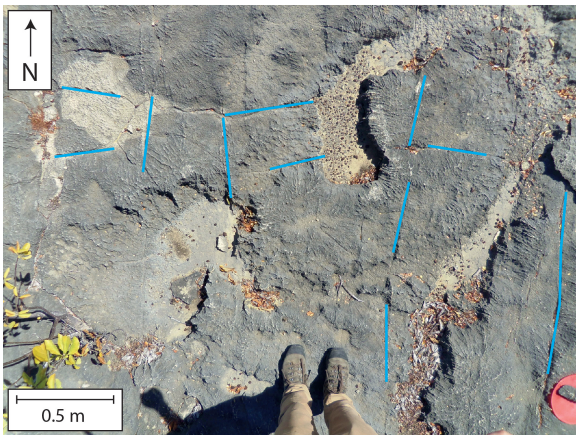

(b) Mode I fractures of predominantly E-W (red) and N-S (yellow) azimuth.

Figure 3.6: Joint fractures of the Jandaira outcrop.

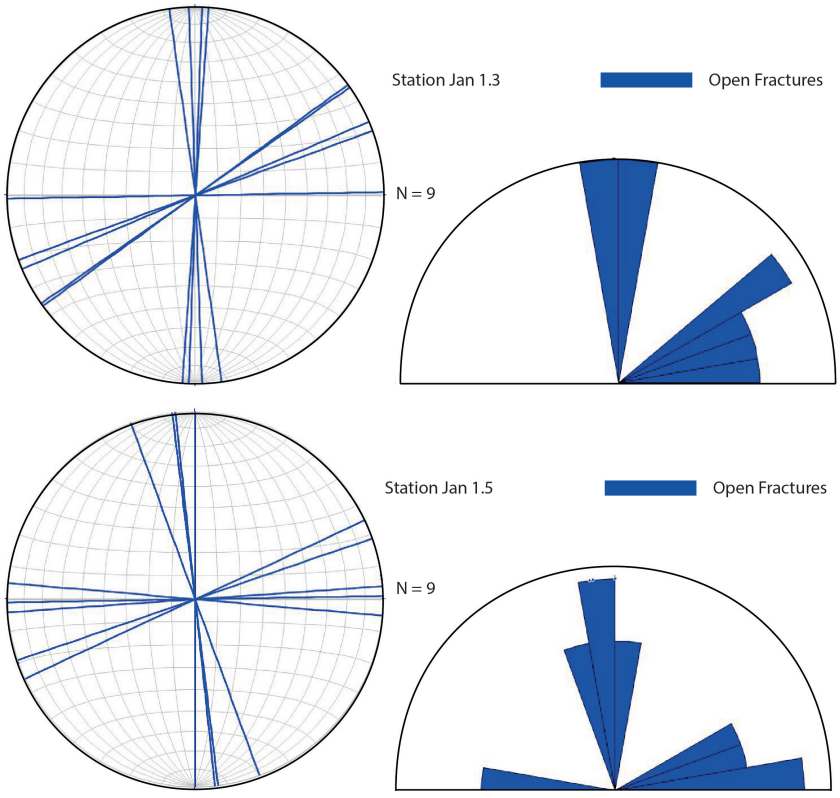

Figure 3.7: Stereoplot (left) and Rose plot (right) of the structural features of the Jandaira outcrop.

3.3. Discussion

3.3.1. Principal stress orientations

Areas examined during this study were located on the edges of the Potiguar basin, with the Sao Geraldo area in the West, the Mossoro area in the North-West and the Jandaira area in the North-East. Structural feature similarities are present throughout the studied areas in the Potiguar basin with similar orientations of open fractures and veins towards both the NW-SE and NE-SW in the West of the Potiguar basin and open fractures oriented towards both the N-S and E-W in the East of the basin. σ_3 of the open fractures and veins are parallel to the opening direction and are therefore taken together. σ_1 is determined as being formed perpendicular to the orientation of vertical stylolite. Vertical stylolite measurements taken by previous authors (Bertotti et al., 2017) have been used for this study. All data is combined and used to examine the regional distribution (figure 3.8). Figure 3.9 and 3.10 depict σ_1 and σ_3 throughout the basin and for the NE-SW and NW-SE compressional episodes, respectively.

For the western part of the Potiguar basin, σ_3 of the two episodes is oriented towards 290 ± 15 degrees NW and 30 ± 20 degrees NE. In the eastern part of the basin, σ_3 of two episodes are oriented towards 340 ± 20 degrees NW and 70 ± 30 degrees NE. The absence of fracturing in other directions indicate a difference of 40-50 degrees of σ_3 in the orientation of the two episodes. Determination of σ_1 was possible in the central and western part of the basin and show σ_1 of two compressional episodes, oriented towards the NW-SE and NE-SW. It is not possible to determine regional variations of σ_1 due to a lack of σ_1 indicators in the eastern part of the basin. Measurements of σ_1 and σ_3 indicate two compressional episodes. One compressional episode is characterized in the west of the basin by a NW-SE oriented σ_1 and a NE-SW oriented σ_3 and in the east of the basin by a E-W oriented σ_3. The other compressional episode is characterized in the west of the basin by a NE-SW oriented σ_1 and a NW-SE oriented σ_3 and in the east of the basin by a N-S oriented σ_3. Measurements of σ_1 in the basin in the West indicate a different orientation when compared to those outside of the basin. For the NE-SW trending fracture systems, 8 out of 13 measurements within the basin show an σ_1 orientation of 0-20 degrees N-S as apposed to the outside the basin, where the general trend is oriented 50-40 degrees towards the NE-SW. For the NW-SE trending fracture systems, this variance is less prevalent. For the DS area, σ_1 is oriented 175 degrees towards the N-S as apposed to the general trend of 130-150 degrees NW-SE outside of the basin.

Author	Outcrop	Station	Measurements	Coordinates		Stress Directions	
						NE-SW	NW-SE
Hameka, de Graaf, van Eijk	Apodi	AP1	31	629916	9381503	32-212	149-329
		AP2	14	648176	9385026	9-189	168-348
		AP3	26	650636	9387810	11-191	150-330
		AP4	27	652108	9388522	31-211	-
		AP5	11	644376	938942	20-200	-
		AP6	43	653815	9390089	15-195	130-310
		AP7	7	649034	9384915	25-205	-
		AP8	11	652064	9388699	10-190	-
		AP9	14	653392	9388629	10-190	-
	DS	DS1	20	660311	9396042	-	175-355
		DS2	9	659893	9392251	10-190	-
		DS3	19	660737	9392361	40-220	-
		DS4	12	660645	9392124	20-200	165-345
	Mossoro	MO1	10	659647	9443139	-	140-320
		MO2	19	659494	9442828	5-185	110-290
		MO3	18	656664	9438819	0-180	130-310
	Acu	AC 1	7	728014	9387949	-	143.1
This Study	Outcrop	Station	Measurements	Northing	Easting	Stress Directions	
						NE-SW	NW-SE
	Mossoro	MO3	1	-5.0781	-37.58738	-	120-300
		MO4	8	-5.02249	-37.56581	50-230	-
		MO5	4	-5.0781	-37.58738	-	140-320
	Sao Geraldo	SGO2	17	-5.28648	-37.88553	40-220	130-310
		SGO3	2	-5.31501	-37.92706	40-220	-
	Jandaira	JAN1.1	11	-5.33209	-36.13585	20-200	170-350
		JAN1.3	10	-5.33217	-36.13024	30-210	-
		JAN1.4	15	-5.3384	-36.1569	30-210	-
		JAN1.5	10	-5.32106	-36.13715	60-240	140-320
		JAN1.6	3	-5.31021	-36.14521	90-270	170-350

Figure 3.8: Measurements taken from outcrops in the Jandaira formation. The orientation of the σ_1 of the two compressional episodes have been determined at each station with the quality of data availible (green is reliable, red is questionable).

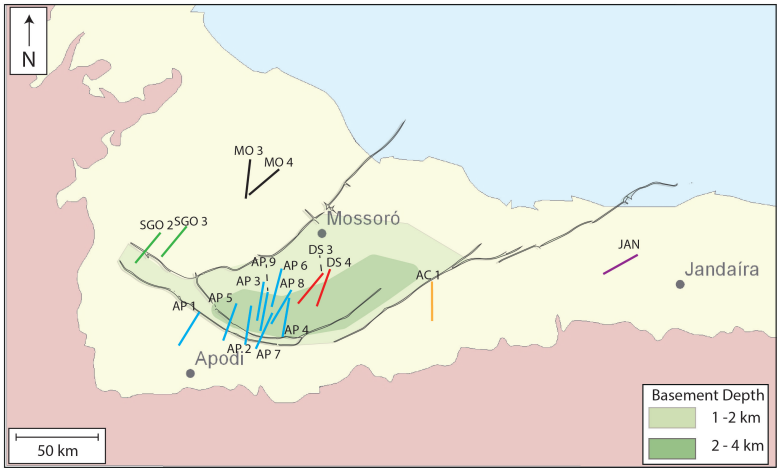

Figure 3.9: Measurements of maximum horizontal stress orientation from NE-SW compression. Indicated are the Sao Geraldo outcrop (green), Mossoro (black), Apodi (blue), DS (red), Acu (orange) and Jandaira (purple).

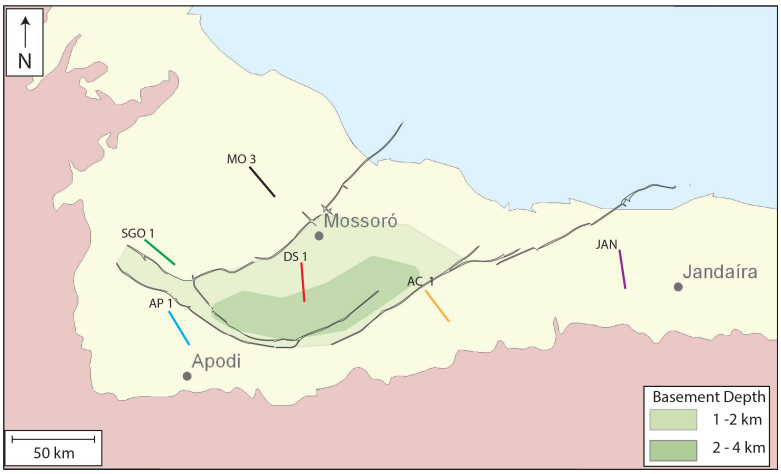

Figure 3.10: Measurements of maximum horizontal stress orientation from NW-SE compression. Indicated are the Sao Geraldo outcrop (green), Mossoro (black), Apodi (blue), DS (red), Acu (orange) and Jandaira (purple).

3.3.2. Relative timing

Rift evolution in the Potiguar basin was controlled by three periods; the initial period of rifting and the associated subsidence and a period of tectonic reactivation in the Late Cretaceous that caused regional uplift (Gurgel et al., 2013). Abutment relations in the Mossoro outcrops showed the presence of at least one compressional episode before deeper burial conditions occurred as the horizontal stylolites overprinted the vertical stylolites and veins. It was not possible to make a distinction between the NE-SW or NW-SE trending sets of vertical stylolites. Previous authors investigated the abutment relations of the Potiguar basin in a more extensive manner where similar observations were made but lacked consistent evidence (de Graaf, 2015; Oskam, 2015). It was also reported that veins overprinted horizontal stylolites (Oskam, 2015). Tectonic reactivation in the Late Cretaceous caused an uplift of the onshore portion of the Potiguar basin and resulted in the present elevated position of the Jandaira. Successively the Jandaira formation was exposed to the following stress fields; a horizontal σ_1 associated with the vertical stylolites during deposition (or shortly thereafter) (1), a vertical σ_1 due to subsidence of the formation and leading to an overprinting of the vertical stylolites by horizontal stylolites (2), reactivation of the basin tectonics leading to fracturing and crystallization of veins that overprint the horizontal stylolites and regional uplift associated with the elevated position of the Jandaira formation (3).

3.3.3. Regional distribution

The orientation of the principal stresses for both horizontal compressional episodes varies throughout the Potiguar basin. As shown above, the orientation between the two episodes of fracturing of the Potiguar basin varies 40-50 degrees. Variations within the basin occur between the western and eastern part of Potiguar basin. Also, variations in σ_1 orientations are present between the inside and outside of the main rift basin as mentioned before. Two scenarios are possible to explain these differences. The first scenario assumes the different parts of the basin are exposed to different stress fields with little local reorientation and the second scenario assumes a regional stress field with larger scale reorientation due to the presence of the rfit basin. The difference in orientation is caused by the basin geometry and the variations between geomechanical properties of the sedimentary infill and crystalline basement (figure 3.11 and 3.12). The second scenario is modelled in the geomechanical chapter of this study.

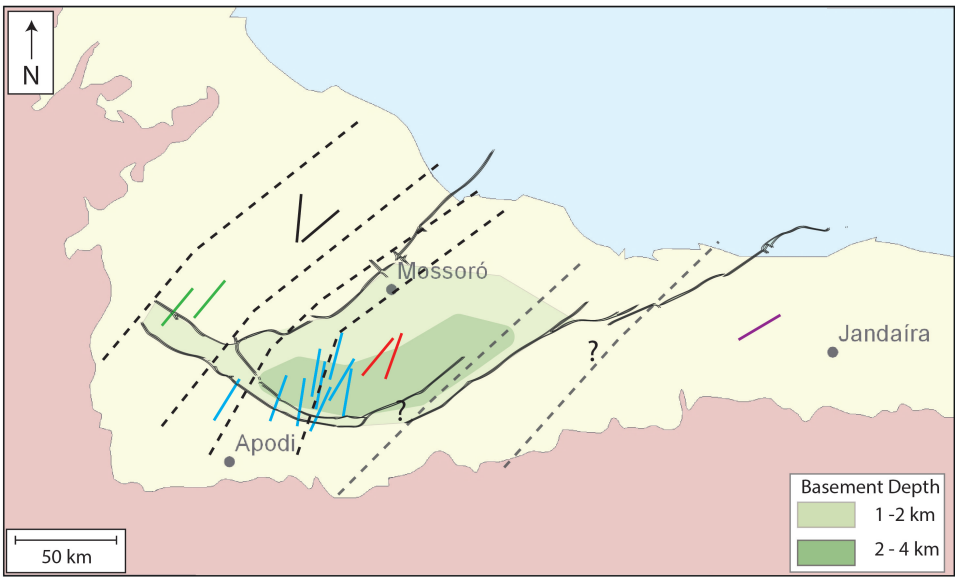

Figure 3.11: Interpolation between the maximum horizontal stress orientation results of figure 3.9. Indicated are the Sao Geraldo outcrop (green), Mossoro (black), Apodi (blue), DS (red), Acu (orange) and Jandaira (purple).

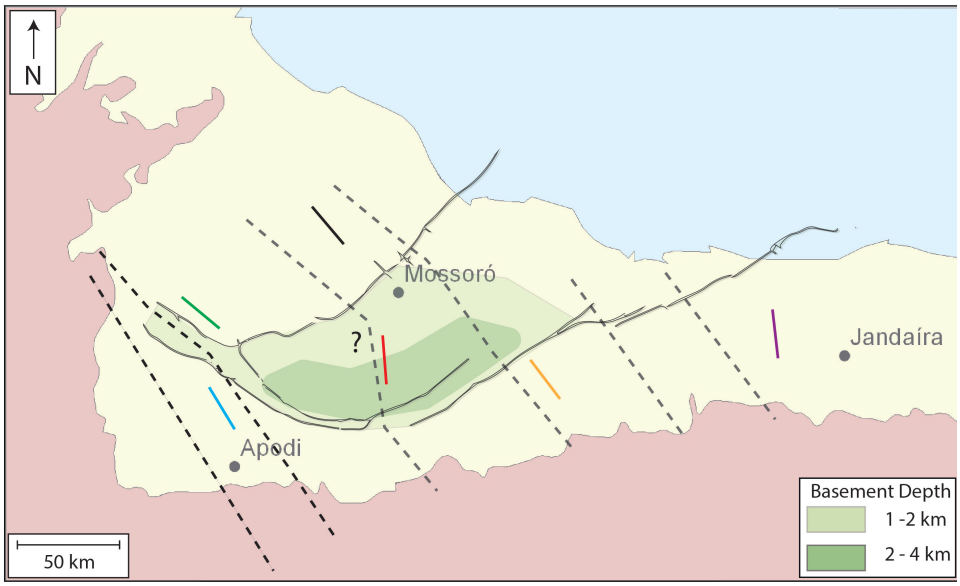

Figure 3.12: Interpolation between the maximum horizontal stress orientation results of figure 3.10. Indicated are the Sao Geraldo outcrop (green), Mossoro (black), Apodi (blue), DS (red), Acu (orange) and Jandaira (purple).

4

Section II - Stylolite analysis

In this section, the aim is to determine the maximum vertical stress and subsequent burial depth that the Jandaira formation has undergone and to investigate regional variations and to further constrain the geomechanical model that is discussed in the next section. To determine the amount of vertical stress on the system, stylolite samples have been examined from the carbonate Jandaira formation at various locations in the Potiguar basin. Fourier-analysis performed on the traces of the stylolites allows for the quantification of the maximum amount of stress exerted on the formation (Schmittbuhl et al., 2004, Ebner, 2009, Koehn et al., 2012). Figure 4.1a and 4.2b show the traces of a horizontal stylolite sample used in this study. Horizontal tectonic forces present during the formation of the horizontal stylolites have an impact on the maximum vertical depth of the horizontal stylolite sample (Bertotti et al., 2017) and these effects have been implemented in the results. Lastly, an indication of the amount of horizontal tectonic force present was calculated using the result from a vertical stylolite trace.

(a) Horizontal stylolites from sample L19 that were used for Fourier transform analysis.

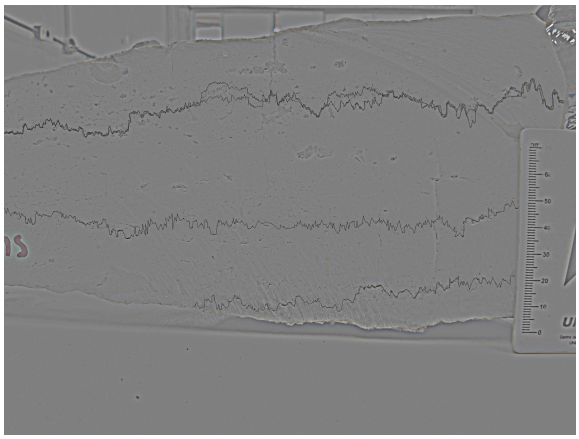

(b) Digitized stylolite trace of L19 Bot. Digitized stylolite trace of L19 Bot. Digitized.

Figure 4.1: Horizontal stylolite trace.

4.1. Method

Stylolites are created by deforming carbonate rocks, where stresses applied on the rocks cause dissolution of calcite and creates serrated surfaces of residual matter with a general orientation perpendicular to the principal stress σ_1. The serrated surfaces of the stylolites are formed in a self-affining manner, where the shape of the stylolite is independent of the resolution at which it is observed but larger samples are preferred in the analysis as it reduces the noise in the signal (Barabási and Stanley, 1995; Meakin, 1998). The creation of the large scale shape is an upscaled, similar version of the formation of the smaller scale shape. The shape of the serrated surface of the stylolites is dominated by two processes; one large-scale process of the larger wavelengths that is dependent on the elastic energy in the system and one smaller- scale process of the smaller wavelengths that is dependent on the surface energy of the system (Schmittbuhl et al., 2004)). By applying Fourier transform on the stylolite traces, these two processes are visible in two trends. The intersection between the two trends is the crossover length and is indicative for the amount of stress applied on the system during deformation. The slope of these trends is represented by $(k) = k^{-1-2H}$, where H stands for the Horst component. The Horst component ranges between 0.3-0.8 for the surface energy regime and between 0.8-1.2 for the elastic regime. Stress applied on a system has an effect on the interaction between both processes and an increase of stress is associated with a decrease of crossover length (in mm^{-1})(Ebner et al., 2009)).

Using the method described by Ebner et al. (2009), the Fourier power spectrum can be constituted over the trace of the stylolite image. With the relation proposed, the amount of stress required to create such a stylolite is determined with the relation between the crossover length and deformation stress (Ebner (2009);

$$(\sigma_{zz}^2) = \frac{\gamma E}{\alpha \beta L_c}$$

Where γ is the surface tension, E is the young's modulus, $\alpha = \frac{1(1+\nu)(1-2\nu)}{3(1-\nu)(1-\nu)}$, $\beta = \frac{2\nu(1-2\nu)}{\pi}$, v is the Poisson's ratio and L_c is the crossover length.

The burial depth is then calculated with $\sigma = \rho g z$. The stresses with this method are subject to gravitational forces and an extension of the equation has been proposed to include horizontal stresses exerted on the system (Rolland et al. (2014));

$$\sigma_x = \sigma_y = \frac{\nu}{1-\nu}\sigma_{zz}$$

Samples have been gathered over the western section of the Potiguar basin from the Mossoro, Apodi and Sao Geraldo outcrops. In total, 35 samples have been collected and cut perpendicular on the stylolite plane in order to clearly distinguish the trace of the stylolite(s) (figure 1a). Out of the 35 rock samples, 6 rock samples were photographed to obtain 9 sub-horizontal traces and 4 sub-vertical traces. The photos of the stylolite traces were then digitized with Photoshop and Matlab (figure 1b) and corrected for scale. Fourier transform is performed on the trace to transform the data from an x-y plane to that of frequency over amplitude, where the Nyquist critical frequency is equal to double the pixel size of the photograph.

(a) Vertical stylolite from sample L24 that is used for Fourier transform analysis.

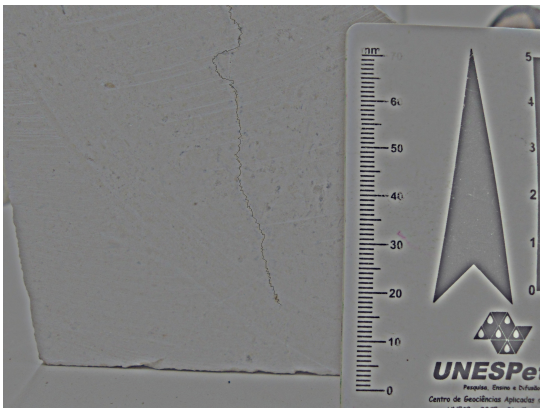

(b) Digitized stylolite trace of L19 Bot. For analysis purposed the trace has been rotated 90 degrees.

Figure 4.2: Vertical stylolite trace.

4.1.1. Tectonic influence

The calculations to determine the amount of stress during the time of formation of the sub-horizontal stylolites were assumed to have occurred during burial with uni-axial stress conditions. As described in previous research (Oskam (2015), Bertotti et al. (2017)) this is likely not the case. Using the transformation of Bertotti et al. (2017), a tectonic force of 10-20 MPa is imposed on the system and a new vertical stress can be calculated that assumes this force to be present during deformation and therefore requiring a higher vertical stress and therefore burial depth to account for the crossover length. The alternate vertical stress required for the stylolite trace formation with tectonic influence is calculated by modifying the equation 1 assuming no anisotropic stress conditions but $\sigma_{yy} = \frac{\nu}{1-\nu}\sigma_{zz} + S_{tect}$ and $\sigma_{xx} = \frac{\nu}{1-\nu}\sigma_{zz} + \frac{\nu}{1-\nu}S_{tect}$;

$$L_c = \frac{\gamma E}{\beta \sigma_{mean} \sigma_{differential}}$$

$$\sigma_{mean} = \frac{\sigma_{zz} + 2\frac{\nu}{1-\nu}\sigma_{zz} + \frac{\nu}{1-\nu}S_{tect} + S_{tect}}{3}$$

$$\sigma_{differential} = \sigma_{zz} - [\frac{\nu}{1-\nu}\sigma_{zz} + \frac{\nu}{1-\nu}S_{tect}]$$

$$L_c = \frac{\gamma E}{\beta \frac{1}{3}(a\sigma_{zz}^2 + b\sigma_{zz} - c)}$$

Where:

$$a = 1 + \frac{\nu}{1-\nu} - 2[\frac{\nu}{1-\nu}]^2$$

$$b = \sigma_{tect} - 3S_{tect}[\frac{\nu}{1-\nu}]^2 - S_{tect}[\frac{\nu}{1-\nu}]$$

$$c = [\frac{\nu}{1-\nu}]^2 S_{tect}^2 - [\frac{\nu}{1-\nu}]^2 S_{tect}^2$$

4.1.2. Rock properties

The parameters used in the various equations that describe the rock properties were taken from Oskam (2015) with maximum and minimum values of respectively (table 1). Further sensitivity analysis was also done using known variations in the rock properties (Schultz, 1993; Gercek, 2006). The amount of stress related to the crossover lengths of all stylolite samples are depicted in table 2. The weighted average is determined by the quality of the data ranging from 1 (bad) to 3 (good) multiplied with the corresponding crossover point (Appendix 1). The definition of bad and good is determined in respect to the Fourier results, where some samples showed only minor differentiation between the smaller and larger wavelengths. For the parameters used in the stress calculation, the averages were used. By implementing the weighted average for each outcrop, the asymmetry of the stress distribution can be approximated and the clear results are better represented. Assuming burial deformation, depth can be determined by $\sigma = \rho g z$ with a density of 2400 kg/m$\hat{3}$. The Fourier transforms of the other all samples is shown in Appendix 2.

Parameters	Surface Tension	Poisson	Young	Alpha	Beta
Max	0,27	0,33	55	0,336	0,071
Min	0,27	0,24	15	0,372	0,079
Average	0,27	0,285	35	0,354	0,075

Figure 4.3: Parameters used for the stress calculations (Schultz, 1993; Gercek, 2006).

4.2. Results

Uni-axial condition for the single trace of L19Bot are displayed in figures 2 and 3. From the Fourier analysis plot of figure 3, two trends can be distinguished. These two lines coincide with trendlines of $y1 = 75x^{-1.8}$ and $y2 = 53.x^{-3.2}$ and are representative for the long- and short wavelengths that dictate the profile of the stylolite. From Schmittbuhl et al. (2004) $P(k) = k^{-1-2H}$ determines the Horst component of the stylolite, where H < 0.8 accounts for the short wavelengths and H > 0.8 for the long wavelengths. The horizontal stylolite of L19 bot therefore coincides with a short wavelength Horst component of 0.4 and a long wavelength Horst component of 1.1. The crossover length is determined by the inverse of the crossover point between both trends, which in this case is 7.0^-1 = 1.43 mm^-1. For the vertical stylolites, the traces were rotated 90 degrees clockwise to accommodate for the Fourier analysis. Figures 4, 5 and 6 depict the digitalization and Fourier analysis of vertical stylolite from sample L24.

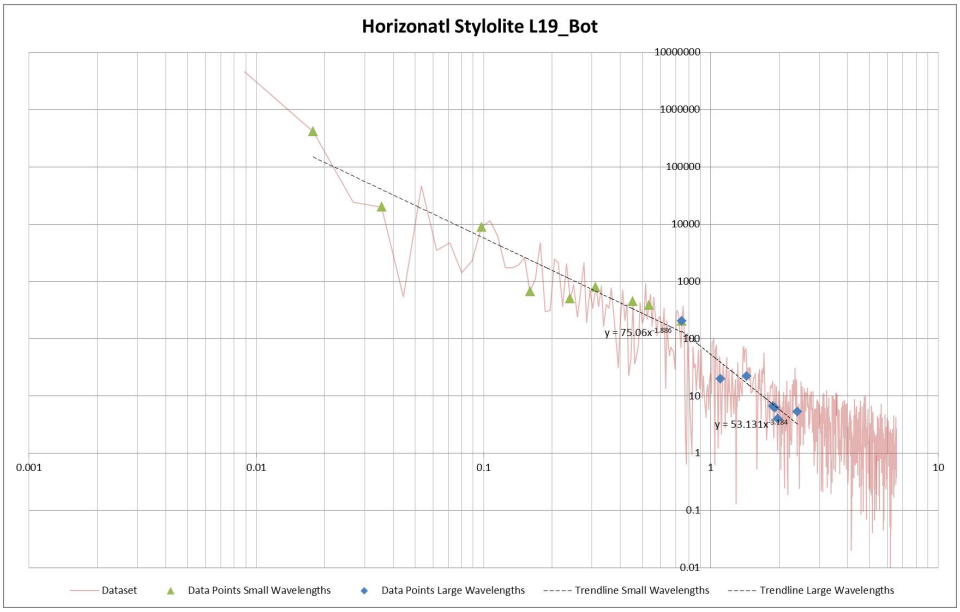

Figure 4.4: Fourier transform executed on the digitized trace of figure 2. The trend lines are visible for the elastic regime (blue diamonds) and the surface tensional regime (green triangles).

Outcrop		Sao Geraldo	Mossoro						Apodi	
Sample		L3	L13	L13_Bot	L14	L19	L19_2	L19_Mid	L19_Bot	L21_Mid	L21_Bot
Sample no.		1	2	3	4	5	6	7	8	9	10
Crossover Point (mm)		0.15	0.5	0.9	0.5	0.6	0.6	0.55	0.75	0.35	0.3
Crossover Length (mm^{-1})		6.67	2	1.11	2	1.67	1.67	1.82	1.33	2.86	3.33
Maximum Vertical Stress (Mpa)	Minimum	4.7	8.7	11.6	8.7	9.5	9.5	9.1	10.6	7.2	6.7
	Average	6.7	12.2	16.4	12.2	13.4	13.4	12.8	15	10.2	9.5
	Maximum	9.1	16.6	22.2	16.6	18.2	18.2	17.4	20.3	13.9	12.8
Maximum Burial Depth (m)	Minimum	201	368	493	368	403	403	386	450	308	285
	Average	285	520	698	520	570	570	545	637	435	403
	Maximum	386	704	945	704	771	771	738	862	589	545

Figure 4.5: Vertical Stresses associated with the crossover lengths for each sample.

The results of the maximum vertical stress and burial depth of all samples is displayed in figure 4.6. Horizontal tectonic stresses of 10, 20 and 30 MPa have been implemented in the calculations and the effects are depicted in figure 4.11b. Here the weighted average of the maximum burial depths of 0, 10, 20 and 30 MPa were used.

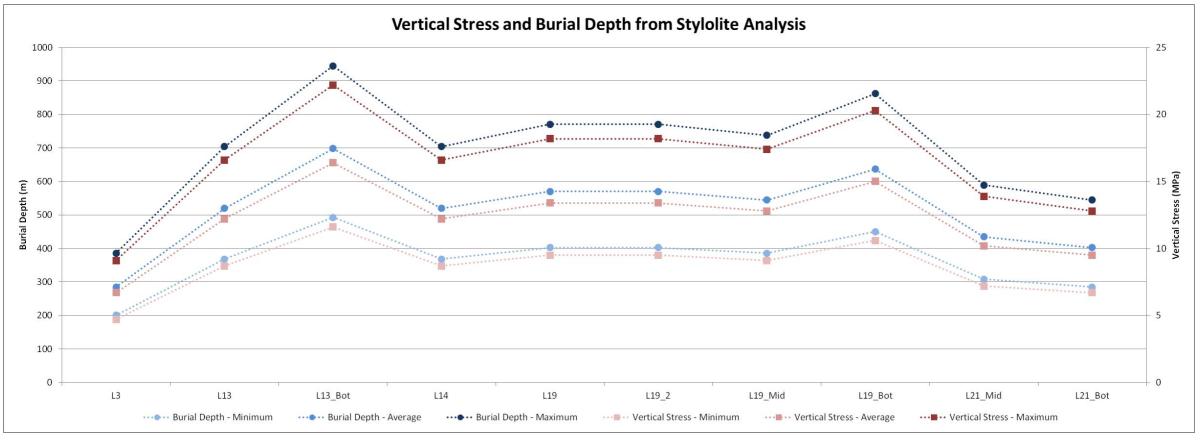

Figure 4.6: Vertical stress and bural depth determination from the horizontal stylolite trace analyses.

Outcrop		Sao Geraldo	Mossoro						Apodi	
Sample		L3	L13	L13_Bot	L14	L19	L19_2	L19_Mid	L19_Bot	L21_Mid	L21_Bot
Maximum burial depth (m)	0 Mpa	290	520	700	520	570	570	550	640	440	400
	10 Mpa	430	620	770	620	660	660	640	720	540	520
with tectonic influence	20 Mpa	700	820	930	820	850	850	840	900	770	750
	30 Mpa	920	1000	1100	1000	1020	1020	1020	1020	970	960

Figure 4.7: The influence of a horizontal tectonic influence of respective 10, 15, 20 and 30 MPa on the weighted average burial depth.

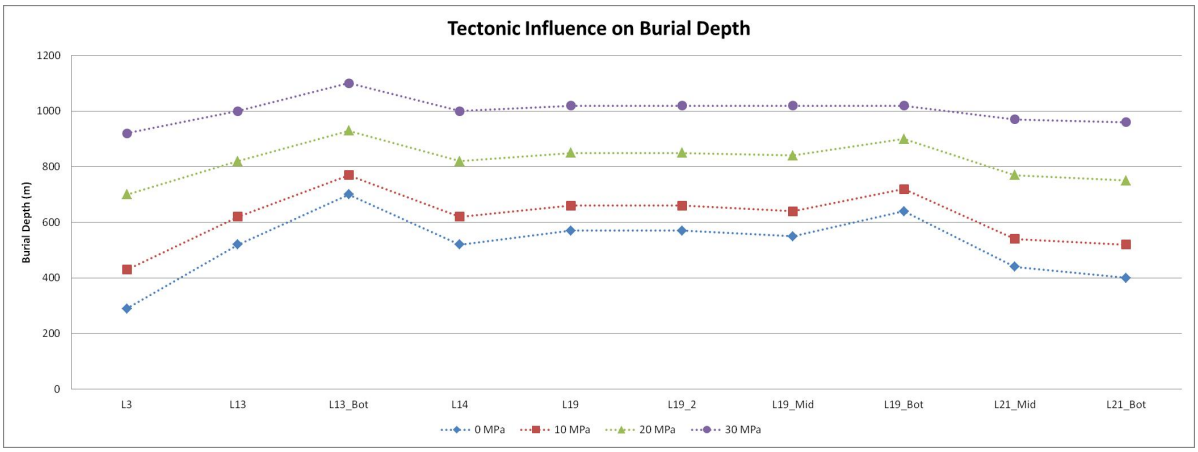

Figure 4.8: Implementation of the tectonic forces of 0, 10, 20 and 30 MPa into the vertical stress calculations.

4.2.1. Sample evaluation

Samples that show the best results, where the distinction between the elastic and surface tensional regimes is easily recognized, are the samples with the longest and well defined traces. Figure 15 shows the results from a “good” and “bad” sample in this respect. In the case of “bad” samples, picking the cross-over point between the two regimes is more difficult to perform. The relative effect of the good and bad samples have been taken into account when determining the stresses.

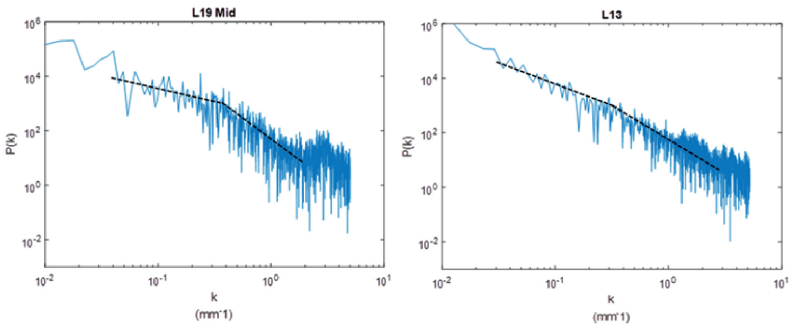

Figure 4.9: An example of a relatively good (left) and a bad (right) Fourier transform result.

4.3. Discussion

For the scenario of no tectonic influence, the vertical stresses calculated from the stylolite traces have not exceeded a maximum of 21 MPa, weighted average of 15 MPa and a minimum of 5 MPa. This coincides with a maximum burial depth 915 m, weighted average 650 m and minimum of 200 m (one sample). Comparing the results of the sub-horizontal stylolites from in this study with a similar study of Oskam (2015), the respective burial depths of the Mossoro and Apodi outcrop are mostly similar for both outcrops, with an exception with the Apodi outcrop, where the new data exhibits the largest variation with previous data (figure 4.10a and 4.10b).

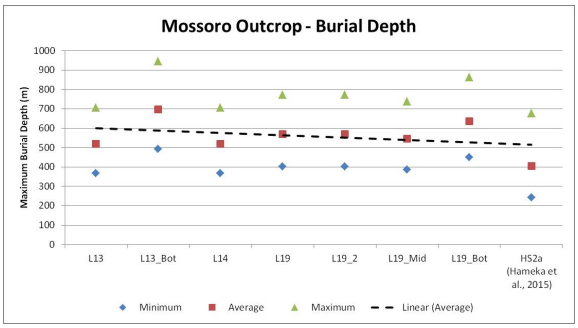

(a) Minimum, weighted average and maximum burial depth at the Mossoro outcrop and the comparison with previous data.

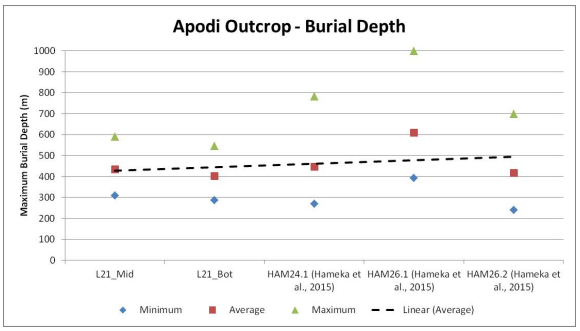

(b) Minimum, weighted average and maximum burial depth at the Apodi outcrop and the comparison with previous data (Oskam (2015)).

Figure 4.10

Taking horizontal tectonic stress into account, the additional equations were solved over the measured crossover lengths of the samples, resulting in figure 4.11b depicting the weighted average burial depths required to produce the stylolite traces with a horizontal tectonic influence of respective 0, 10, 20 and 30 MPa (figure 11). Similar to the results of the uni-axial conditions, regional burial depths are between 10 and 27 % for a horizontal tectonic stress of 10 and 30 MPa, where the decrease in the spread among the samples reduces as the tectonic stresses increase. Appendix D contains tables of the values used for the tectonic stress calculations for each sample and outcrop.

4.3.1. Sensitivity analysis

Sensitivity analysis is performed on the base case of no tectonic influence, where the rock properties used to calculate both the maximum vertical stress and maximum burial depth were varied (figure 4.11a and 4.11b). For both the vertical stress and burial depth the cross-over point, Poisson ratio and Young modulus were varied and for the burial depth the density was also varied. The cross-over point and the young modulus were the largest contributors for uncertainty, with the cross-over point exhibiting a deviation of up to 10 % and the Young Modulus of up to 30 %. Variation in the cross-over point is expected, as a difference of for instance 0.2 and 0.3 accounts for a change of a third in the cross-over length ($0.3^{-1}/0.2^{-1}$). The variation in the Young Modulus is due to the large spread between the minimum and maximum values (15 and 55). The spread

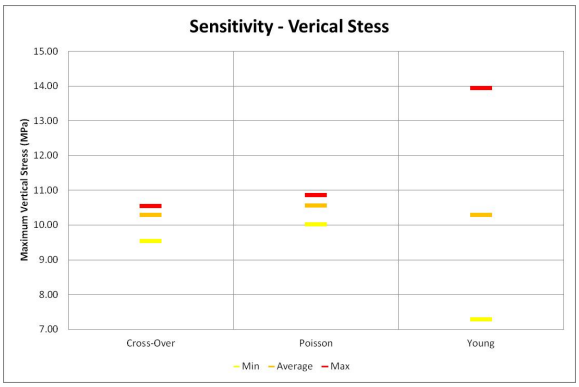

(a) Minimum (yellow), average (orange) and maximum (red) values of the rock properties used in the vertical stress calculations.

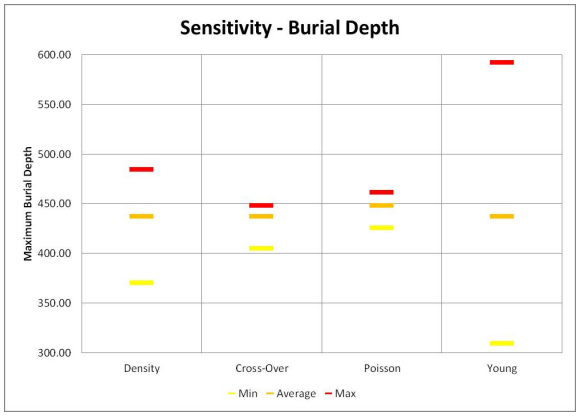

(b) Minimum (yellow), average (orange) and maximum (red) values of the rock properties used in the vertical stress calculations.

between the minimum and average is understandable as the sedimentary fill of the Potiguar ranges between the finer grained clays and siltstones which account for a low Young Modulus and the durable carbonates of the Jandaira formation that have a higher Young Modulus. The maximum of 55 MPa , however, might be too high as no metamorphic rocks are present and the burial depths are not extreme.

4.3.2. Vertical stylolites

The vertical stylolites measured in this study show mixed results. Compared with the results from the horizontal stylolites, the behaviour of vertical stylolite L24-V1 is similar but the others do not show any cross-over point in the Fourier Analysis. The vertical stylolites found in this study are generally less visible and short and because of this the Fourier analysis does not run for over a sufficiently long trace resulting in anomalies and more uncertainty. From the clear sample, the amount of stress is determined in the same manner as the horizontal stylolites and assumes uni-axial compression. Results showed a weighted average horizontal stresses at the Apodi outcrop of around 13 MPa and with a maximum horizontal stress of up to 20 MPa. The sample was from an unoriented sample and an orientation of $\sigma_{H,max}$ is not possible.

Because one sample was usable for Fourier analysis, any conclusions regarding horizontal tectonic forces are preliminary. Nevertheless, these results could be taken as an archor point in regards to the amount of maximum horizontal stress exerted on the formation at shallow depths. Throughout the outcrops where the vertical stylolites were found the horizontal stylolites were more abundant and the vertical stylolites proved difficult to extract. From the vertical stylolites that we were able to obtain, only one trace proved to have a defined trace for Fourier analysis. The state of the formation of the vertical stylolites must therefore have been (much) larger than the well-defined stylolite trace of L24-V1 and a maximum horizontal compression of 13 MPa.

4.3.3. Regional stress distribution

Results from the Fourier analysis on horizontal stylolite traces show a consistency in maximum burial depth throughout the examined samples. Implementation of the presence of a horizontal tectonic stress during the formation of the horizontal stylolites causes an increase in the burial depth and a decrease in the spread throughout the samples. The maximum burial depth of the weighted average is around 600 meters for the uni-axial scenario, 700 meters for the scenario of 10 MPa horizontal tectonic stress, 850 meters for the scenario of 20 MPa horizontal tectonic stress and 1000 meters for the scenario of 30 MPa horizontal tectonic stress. The results gathered in this study show a limited amount of spatial variation in burial depth and indicate a scenario of regional subsidence.

5

Section III - Basin modelling

This section aims to construct a geomechanical basin model of the Potiguar basin and to model the distribution of the principal stresses. To construct the geomechanical model a geological model is created using the basin geometry, fault characteristics and sedimentary formation data of the basin. Scenarios of horizontal tectonic influence were modelled by implementing geomechanical properties and horizontal stress ratios (relative to the vertical stress). In this study the following scenarios were modelled; a base case scenario of uni-axial conditions, horizontal compressional stress conditions of 10 and 20 MPa and the current state of stress. The results from the previous sections concerning principal stress orientations and magnitudes were implemented in the geomechanical model to further constrain the boundary conditions. The present day state of stress conditions (after Reis et al., 2013) were applied on the model and the distribution of the principal stress orientations and magnitudes have been calculated.

5.0.1. Basin geometry database

The basin geometry and lithology have been studied for a long time and therefore much is known. The basement consist of pre-rift crystalline rocks and are outcropping on the west, south and east side of the Potiguar basin. Through gravity anomaly maps of the Potiguar basin and seismic imaging the depth of the basement and the extent of the southern and eastern bounding faults were determined (figure 5.1a) (de Costa (2015)). The sedimentary formations in the Potiguar basin consist of the syn-rift Pendencia formation, the post-rift siliclastic Acu formation and the post-rift carbonate Jandaira formation. The extent of these formations through the basin is well defined by outcrop studies and well logs (Sampaio & Schaller, 1968; Bertani, 1987; Matos, 1992). Combining the geological map of outcropping formations with their respective isopach maps (figure 5.1b) allowed for the reconstruction of the extent of the sedimentary formations throughout the basin.

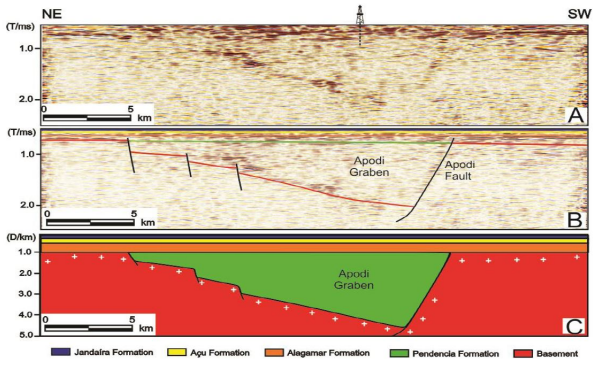

(a) Seismic and interpreted image of the sedimentary facies and the basement with the estimated fault length.

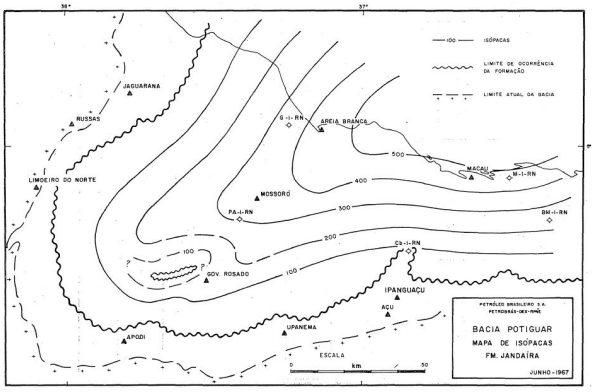

(b) Isopach map of the carbonate Jandaira formation.

Figure 5.1: Figures that were used to construct the basin geometry, the top surfaces of the sedimentary facies and the basement surface.

5.1. Method

The geolocial model is constructed using the formational database described before using SKUA-GOCAD geological modelling software. Surfaces of each formation were generated and then imported into JewelSuite geomechanical modelling software. From all surfaces, a finite element grid is constructed in the size of the basin and geomechanical properties are assigned to the formations (figure 5.2a)(Schultz,1993;Gercek,2007). A number of scenarios were modelled after various magnitudes and orientations of horizontal tectonic influence. In order to implement the horizontal tectonic stress into the model, maximum and minimum horizontal stress ratio's (SHmax and SHmin) relative to the vertical stress (Sv) were determined. Vertical stress was calculated with ρgz in the middle of the basin using the same method as in the stylolite section with the following stress matrix. Implementing horizontal tectonic influences of 10 and 20 MPa with the stress matrix allowed for the calculation of the SHmax and SHmin ratios (figure 5.3).

$$\begin{matrix} \frac{v}{1-v}\rho gz + \frac{v}{1-v}S_{tect} & 0 & 0 \\ 0 & \frac{v}{1-v}\rho gz + S_{tect} & 0 \\ 0 & 0 & \rho gz \end{matrix}$$

Formation	Density (kg/m3)	Young's modulus (Pa)	Poisson ratio
Jandaira	2400	30000	0.3
Acu	2200	30000	0.3
Pendencia	2400	30000	0.3
Basement	3000	60000	0.2

(a) Geomechanical properties used for scenarios 1, 2, 3 and 5 of the geomechanical basin model (Schultz,1993;Gercek, 2007).

Formation	Density (kg/m3)	Young's modulus (Pa)	Poisson ratio
Jandaira	2400	45000	0.3
Acu	2200	30000	0.4
Pendencia	2400	40000	0.4
Basement	3000	60000	0.1

(b) Geomechanical properties of scenario 4, amplifiying the differences of the geomechanical properties from figure 5.2a.

Figure 5.2

Principal Stress - Absolute								
Depth	Density	Sv	Actual Sv	Relative Differenc	T =	10	T =	20
(m)	(kg/m3)	(Mpa)	(Mpa)	e	SH,max	SH,min	SH,max	SH,min
100	2400	5.35E+06	4.30E+06	0.80	1.18E+07	6.13E+06	2.18E+07	1.04E+07
200	2400	7.71E+06	5.60E+06	0.73	1.24E+07	6.69E+06	2.24E+07	1.10E+07
400	2400	1.24E+07	8.20E+06	0.66	1.35E+07	7.80E+06	2.35E+07	1.21E+07
500	2200	1.46E+07	9.50E+06	0.65	1.41E+07	8.36E+06	2.41E+07	1.26E+07
1000	2200	2.54E+07	1.60E+07	0.63	1.69E+07	1.11E+07	2.69E+07	1.54E+07
1500	2200	3.62E+07	2.25E+07	0.62	1.96E+07	1.39E+07	2.96E+07	1.82E+07
2000	2200	4.69E+07	2.90E+07	0.62	2.24E+07	1.67E+07	3.24E+07	2.10E+07
2500	2400	5.87E+07	3.55E+07	0.60	2.52E+07	1.95E+07	3.52E+07	2.38E+07
3000	2400	7.05E+07	4.20E+07	0.60	2.80E+07	2.23E+07	3.80E+07	2.66E+07
3500	2400	8.23E+07	5.30E+07	0.64	3.27E+07	2.70E+07	4.27E+07	3.13E+07
4000	3000	9.70E+07	6.40E+07	0.66	3.74E+07	3.17E+07	4.74E+07	3.60E+07
4500	3000	1.12E+08	7.50E+07	0.67	4.21E+07	3.64E+07	5.21E+07	4.07E+07
5000	3000	1.26E+08	8.60E+07	0.68	4.69E+07	4.11E+07	5.69E+07	4.54E+07

Principal Stress - Ratio						
Depth	T = 10 Mpa			T = 20 Mpa		
(m)	Sv	SH,max	SH,min	Sv	SH,max	SH,min
100	0.36	2.75	0.52	0.25	5.08	0.48
200	0.45	2.21	0.54	0.34	4.00	0.49
400	0.61	1.65	0.58	0.53	2.87	0.51
500	0.68	1.48	0.59	0.61	2.53	0.53
1000	0.95	1.05	0.66	0.94	1.68	0.57
1500	1.15	0.87	0.62	1.22	1.32	0.61
2000	1.29	0.77	0.58	1.45	1.12	0.65
2500	1.41	0.71	0.55	1.67	0.99	0.67
3000	1.50	0.67	0.53	1.86	0.90	0.63
3500	1.62	0.62	0.51	1.93	0.81	0.59
4000	1.71	0.58	0.50	2.04	0.74	0.56
4500	1.78	0.56	0.49	2.14	0.70	0.54
5000	1.84	0.54	0.48	2.22	0.66	0.53

Figure 5.3: Lithostratigraphic pressure gradient and the actual pressure gradient from the model. SHmax:Sv and SHmin:Sv ratios were calculated from the pressure gradient of the model.

Five scenarios were implemented for geomechanical modelling (figure 5.4). Scenario 1 was the base case scenario, where uni-axial burial conditions were considerred and the SHmax and SHmin ratios were equal. In scenario 2, horizontal tectonic influence of 10 MPa was applied on the model from 30 degrees NE-SW (scenario 2a) and 0 degrees N-S (scenario 2b). In scenario 3, the horizontal tectonic influence is 20 MPa for both the NE-SW (scenario 3a) and N-S (scenario 3b) direction. Scenario 4 covers the effect of the geomechanical properties on the results and the differences between the formations were amplified (figure 5.8). For this scenario, a horizontal tectonic influence of 10 MPa was applied from the N-S direction. Scenario 5 was modelled after the current state of stress. The SHmax and SHmin ratios of 1.154 was taken between 0.5 and 2.0 km and the 1.396 was taken between 2.5 and 4.0 km (Reis et al, 2013).

Scenario	Tectonic Influence (Mpa)	Orientation (°)	Geomechanical Properties
1	0	0	Fig. 5.2a
2	10	0/30	Fig. 5.2a
3	20	0/30	Fig. 5.2a
4	10	0	Fig. 5.2b
5	0	90	Fig. 5.2a

Figure 5.4: Lithostratigraphic pressure gradient and the actual pressure gradient from the model. SHmax:Sv and SHmin:Sv ratios were calculated from the pressure gradient of the model.

5.2. Results

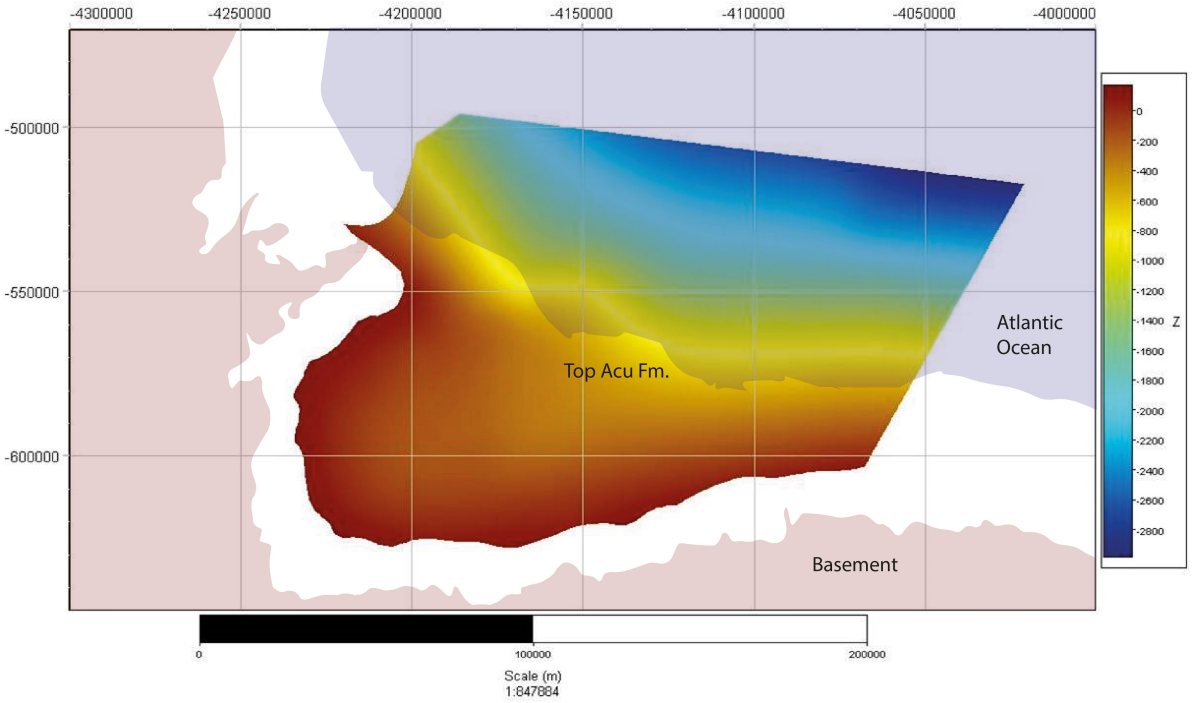

Figure 5.5: Top surface of the Acu formation. The overlay also indicates the crystalline basement in red and the Atlantic ocean in blue.

5.2.1. Geological and geomechanical model

Construction of the formational surfaces was performed with the SKUA-GOCAD geological modelling software. The tops of the Jandaira formation, Acu formation (figure 5.5), Pendencia formation and the basement were combined for the geological model of the Potiguar basin (figure 5.7a). In the geological model, the average thickness of the Jandaira formation is 500 meters and reaches thicknesses of up to 1200 meters in the Northern, offshore, section. The Acu formation has an average thickness of 700 m and reaches thicknesses of

up to 1500 meters in the North. The syn-rift Pendencia formation is situated in the middle of the main rifting basin and reaches up to 3500 meters in thickness. The Pendencia formation is not present outside the main rifting area in the central offshore Potiguar basin. However, it was not possible to implement two erosional surfaces to correctly represent this. In the basin model, the Pendencia formation extends towards the offshore portion of the Potiguar basin. Large faults are present in the Potiguar basin with lengths of up to 4 km but these have not been implemented into the model because of the difficulties that arose with the software. Instead, the basement and Pendencia formation were modified to reflect the the geometry of the faults. For all SKUA-GOCAD and JewelSuite visualizations the depth was exaggerated with a ratio of 1:10 to better reflect the basin geometry.

The surfaces of the formations were imported into JewelSuite geomechanical software to create a finite element grid used for geomechanical modelling. The formations were interpolated over the imported surfaces in the area of the basin to create a finite element 3D grid and 3D mesh which created some anomalies along the fringes of the formational surfaces. Figures 5.6a and 5.6b show the difference of the Pendencia formation between the constructed SKUA-GOCAD surface and the interpolated JewelSuite surface. Interpolation functions could not be set to include the erosional effects and this resulted in a basin wide presence of the Jandaira, Acu and Pendencia formation. In the main rifting basin where all the formations are present, the depth of the JewelSuite surfaces were similar to the SKUA-GOCAD surfaces. This led to the cropping of the 3D Grid to an area of 100 x 70 x 5 km in the central rifting basin (figure 5.7b).

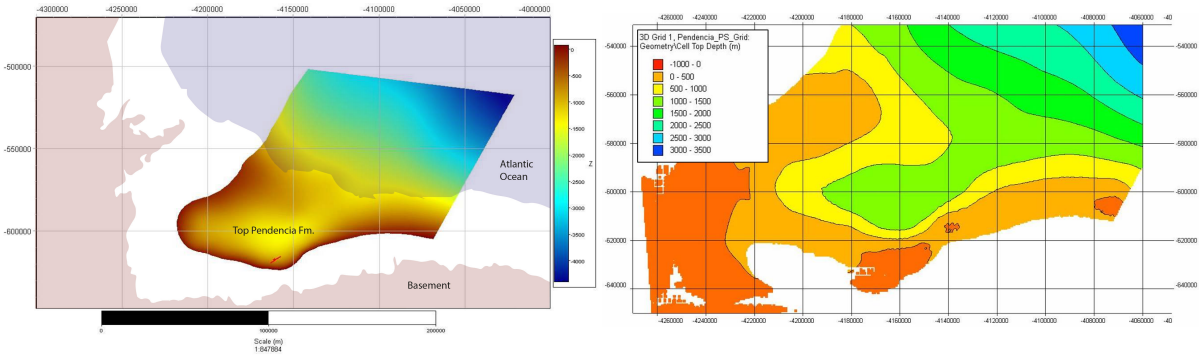

(a) Top surface of the Pendencia formation. Constructed with SKUA-GOCAD geological modelling software.

(b) Top surface of the Pendencia formation. Imported into and interpolated with JewelSuite geomechanical software.

Figure 5.6: The resulting surfaces of the top of the Pendencia formation for the two modelling softwares. Complications with both softwares led to interpolation anomalies.

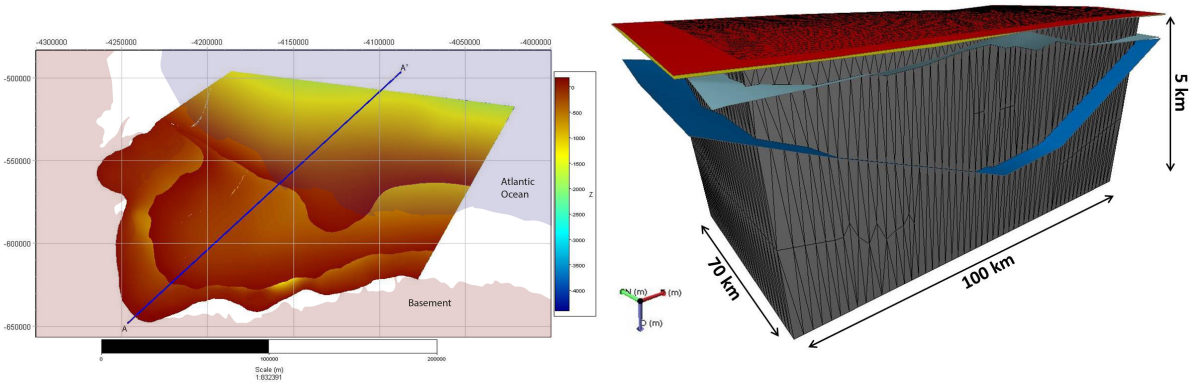

(a) Combined map of the top surfaces in the Potiguar basin model of the SKUA-GOCAD model.

(b) 3D mesh used for the geomechanical modelling in this section.

Figure 5.7: Combined maps of the Potiguar basin model for the two modelling softwares.

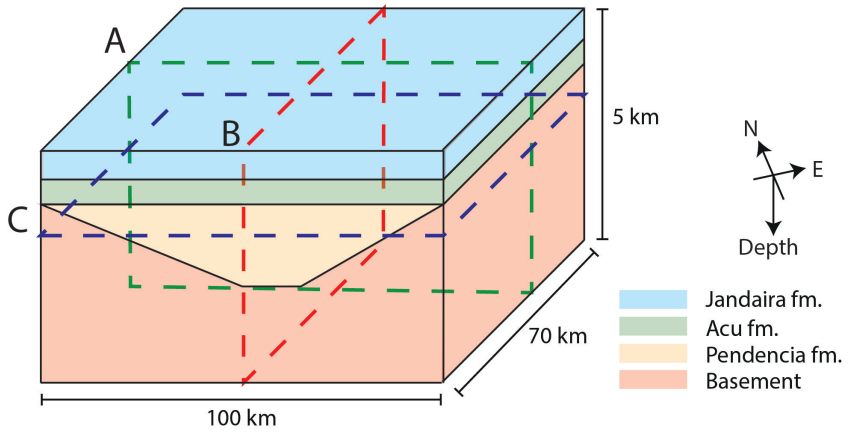

Figure 5.8: Schematic figure of all the elements in the geomechanical model. Cross section A is taken over the length of the model at the middle of the rift, cross section B is taken over the width of the model at the middle of the rift and plane C is taken at a depth of 2000 meters.

5.2.2. Scenario 1 - Uni-axial stress conditions

For the first scenario, uni-axial stress conditions were present. The SHmax:Sv and SHmin:Sv ratios were equal at $\frac{\nu}{1-\nu}$. This scenario not representative for a time period of the Potiguar basin but it was generated to examine the vertical stress distribution throughout the basin without the influence of an external tectonic force. Figures 5.9a and 5.9b depict the σ_1 in cross sections of the central rift and through the length and width of the model. The geology of the basin in the same cross sections is depicted in figure 5.8. From the results is seen that the principal stresses follow the geometry of the basin (figure 5.9a). In the middle of the basin stress magnitudes show lower stress magnitudes when compared to the fringes on the left and right. Increasing depth causes an increase in the basin-wide difference up to the deepest part of the basin, related to the total overburden. After this point, the difference remains the same and does not increase in depth. Over the length of the basin the stress magnitudes are more uniform, with slight changes (figure 5.9b).

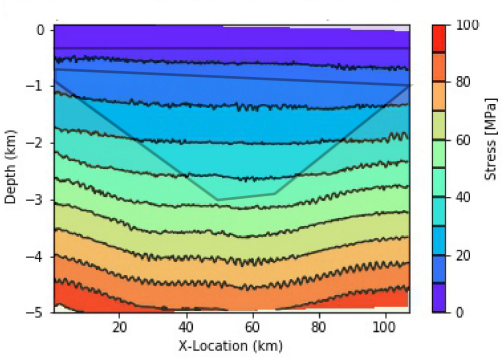

(a) Principal stress σ_1 displayed on plane A. Outlined from top to bottom in the figure are tops of; the Jandaira formation, Acu formation, Pendencia formation and Basement.

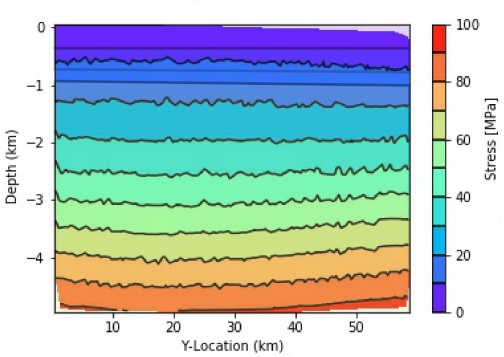

(b) Principal stress σ_1 displayed on plane B. Outlined from top to bottom in the figure are tops of; the Jandaira formation, Acu formation, Pendencia formation and Basement.

Figure 5.9: Principal stress σ_1 under burial conditions.

5.2.3. Scenario 2 - 10 MPa tectonic influence

Scenario 2 and 3 concern the tectonic influence on the state of stress in the Potiguar basin. For scenario 2, 10 MPa compressional stress is imposed on the system with an orientation of maximum horizontal stress (SHmax) of 0 and 30 degrees. Figures 5.10a and 5.10b show the orientation of the horizontal principal stresses at a depth of 2000 meters for these two orientations. Figures 5.11a and 5.11b show the distribution of σ_1 through a cross section over the length of the model for the two orientations.

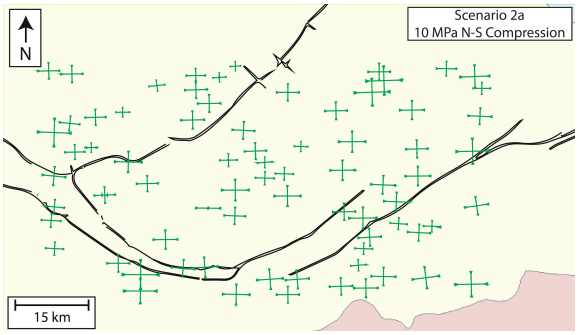

(a) Orientation of the horizontal principal stresses under 10 MPa N-S compression displayed on plane C.

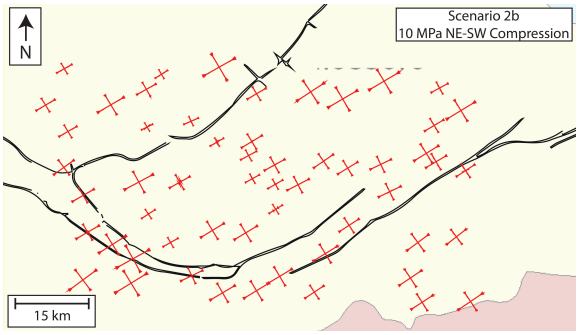

(b) Orientation of the horizontal principal stresses under 10 MPa NE-SW compression displayed on plane C.

Figure 5.10: Orientations of the horizontal principal stresses in scenario 2 conditions.

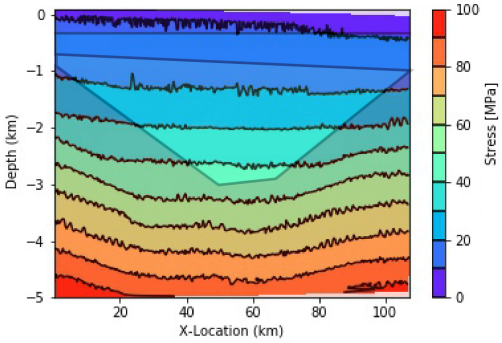

(a) Principal stress σ_1 under 10 MPa N-S compression displayed on plane A. Outlined from top to bottom in the figure are tops of; the Jandaira formation, Acu formation, Pendencia formation and Basement.

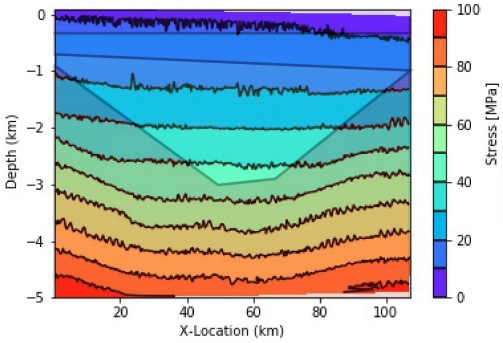

(b) Principal stress σ_1 under 10 MPa NE-SW compression displayed on plane A. Outlined from top to bottom in the figure are tops of; the Jandaira formation, Acu formation, Pendencia formation and Basement.

Figure 5.11: Principal stress σ_1 in scenario 2 conditions.

Minor changes in the orientation of the horizontal principal stresses are visible in the images with slight rotations in orientation towards the contact at the fault between the sedimentary facies and basement where the difference in geomechanical properties is largest (figures 5.10a and 5.10b). In the figures 5.11a and 5.11b, the distribution of σ_1 over the width of the basin is shown and exhibit similar behavior with basin difference and overburden effects. The effects of the horizontal tectonic stress is visible in the top 2 kilometers, where σ_1 is the maximum horizontal stress up to 1.5 km and σ_1 changes to a vertical orientation.

5.2.4. Scenario 3 - 20 MPa tectonic influence

In scenario 3, 20 MPa compressional stress is imposed on the system with an orientation of maximum horizontal stress (SHmax) of 0 and 30 degrees. The orientation of the horizontal principal stresses is shown in figures 5.12a and 5.12b for the two maximum horizontal stress orientations.

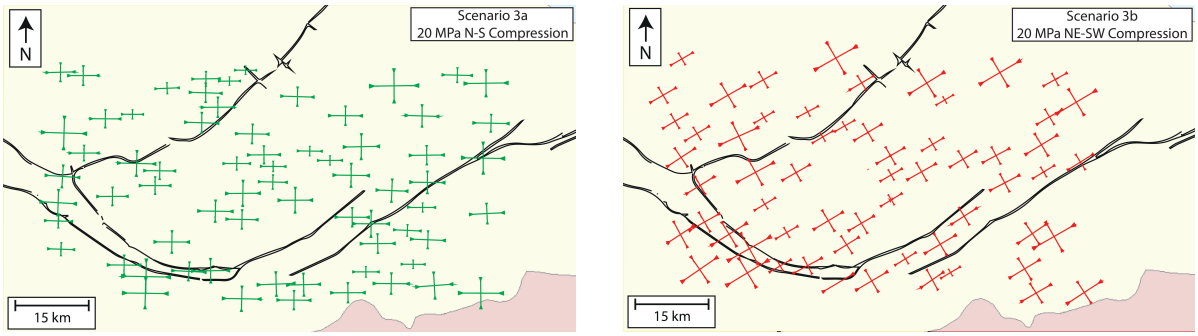

(a) Orientation of the horizontal principal stresses under 20 MPa N-S compression displayed on plane C.

(b) Orientation of the horizontal principal stresses under 20 MPa NE-SW compression displayed on plane C.

Figure 5.12: Orientations of the horizontal principal stresses in scenario 3 conditions.

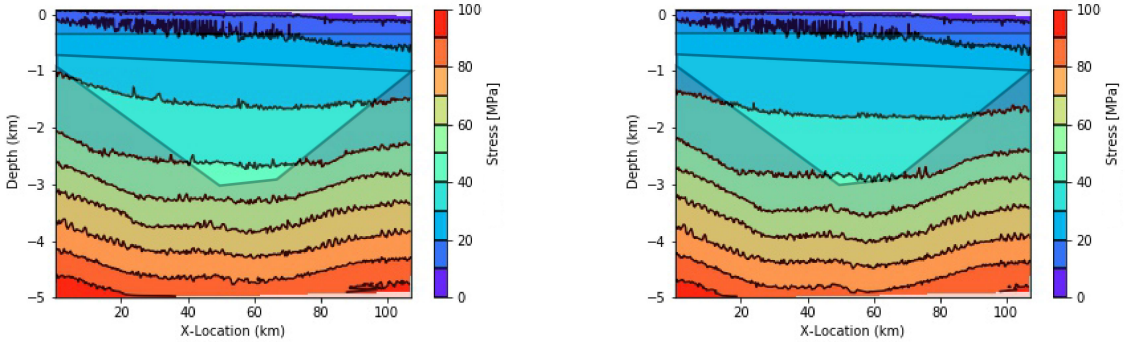

(a) Principal stress σ_1 under 20 MPa N-S compressiondisplayed on plane A. Outlined from top to bottom in the figure are tops of; the Jandaira formation, Acu formation, Pendencia formation and Basement.

(b) Principal stress σ_1 under 20 MPa NE-SW compression displayed on plane A. Outlined from top to bottom in the figure are tops of; the Jandaira formation, Acu formation, Pendencia formation and Basement.

Figure 5.13: Principal stress σ_1 in scenario 3 conditions.

The results of scenarios 3a and 3b are depicted with the orientation of the horizontal principal stresses (figures 5.12a and 5.12b) and stress magnitudes (figures 5.13a and 5.13b). The re-orientation effect towards the formation boundaries as seen in scenario 2a and 2b is less visible and the orientation of the horizontal principal stresses is dominated by the tectonic stress. Stress magnitudes of σ_1 show similar behaviour to scenarios 1, 2a and 2b, with overburden effects between the inside and outside of the basin. The effects of the horizontal stress continue to a deeper depth in the scenarios 3a and 3b and the change between a horizontal σ_1 to a vertical σ_1 occurs at 2.5 km depth.

5.2.5. Scenario 4 - Geomechanical property variance

Scenario 4 consists of scenario 2 (10 MPa N-S compression) with an amplified geomechanical property difference between the sedimentary facies and the basement (figures 5.14a and 5.14b). The geomechanical properties are displayed in figure 5.8. In comparison with scenario 2, the orientation of the horizontal principal stresses is more strongly affected by the basin geometry. Reorientation is most visible at the deeper depths and around the formational boundaries close to the fault where the difference between the geomechanical properties is largest (figure 5.14b).

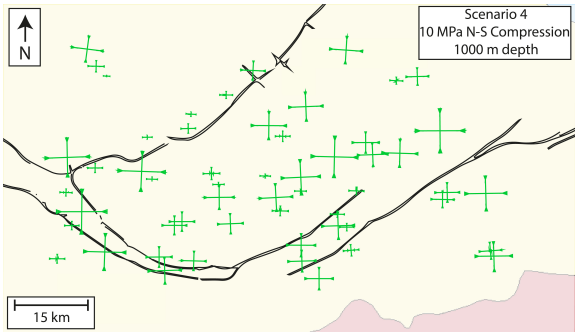

(a) Orientation of the horizontal principal stresses under scenario 4 conditions on plane C. Depth of 1000 meters.

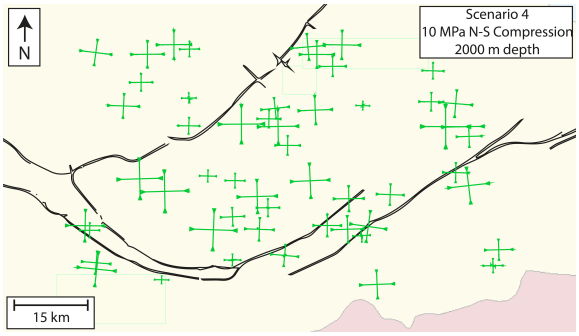

(b) Orientation of the horizontal principal stresses under scenario 4 conditions on plane C. Depth of 2000 meters.

Figure 5.14: Orientations of the horizontal principal stresses in scenario 4 conditions.

5.2.6. Scenario 5 - Present day state of stress

Scenario 4 consists of the present day state of stress and implements SHmax:SHmin ratios of 1.154 for depths between 0.5 and 2.0 km and 1.398 for depths between 2.5 and 4.0 km determined from borehole breakouts in the Potiguar basin (Reis et al., 2013). The orientation of maximum horizontal stress is taken at 90 degrees as this is the dominant orientation in the central and western part of the basin (Reis et al., 2013). Figure 5.15 depicts the orientations of the horizontal principal stresses.

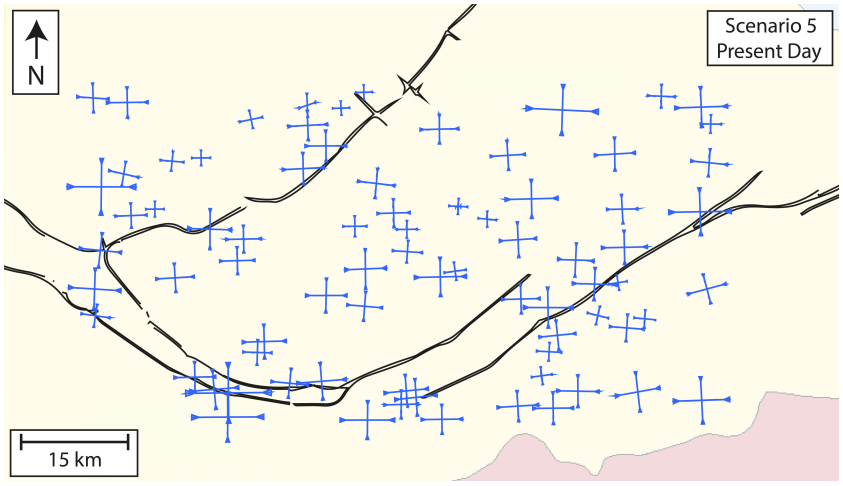

Figure 5.15: Orientation of the horizontal principal stresses in the present day state of stress displayed on plane C.

In the present day scenario, no uniform horizontal tectonic stress was applied on the model. The results show a larger change in orientation than the previous scenarios. But the lack of dominant horizontal stress direction and the coarse grid of the model provides more uncertainty.

5.3. Discussion

5.3.1. Vertical stress mismatch

The $\sigma_{H,max}$:σ_v and $\sigma_{H,min}$:σ_v ratios were calculated using the lithostatic pressure gradient of $\rho g z$ and the stress tensor displayed in the methods section. However, the lithostatic gradient observed in the geomechanical model is inconsistent with the calculated values. The values from the geomechanical model consistently lie between 20 and 40 % below the expected values. Altering the boundary conditions of the ratios did not relieve the problems. The difference between the resulting and expected values seems to be related to geomechanical differences between the sedimentary facies and the basement, where the difference decreased up to 3 km and increased thereafter (figure 5.3). For the determination of the $\sigma_{H,max}$:σ_v and $\sigma_{H,min}$:σ_v calculations, the vertical stresses from the geomechanical model were taken. The pressure-depth plots of the geomechanical model for scenarios 1, 2 and 3 of the initial 3 km are displayed in figures 5.16a, 5.16b and 5.16c.

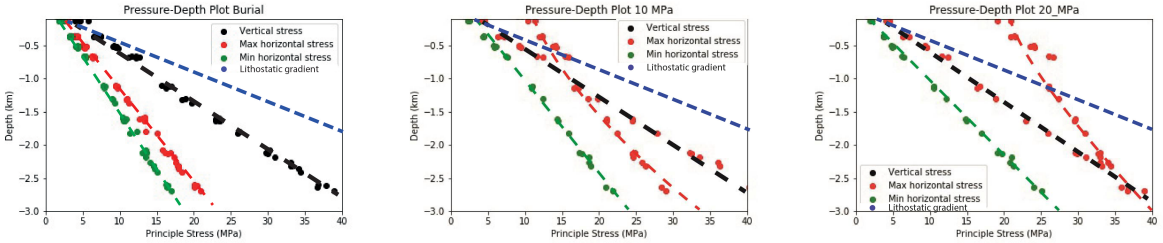

(a) Pressure-Depth plot from modelling with burial, uni-axial conditions.

(b) Pressure-Depth plot from the first tectonic scenario of 10 MPa horizontal compression.

(c) Pressure-Depth plot from the second tectonic scenario of 20 MPa horizontal compression.

Figure 5.16: Pressure-Depth plots of the three tectonic scenarios.

5.3.2. Principal stress orientations

The results from the outcrop section showed that two separate compressional tectonic episodes were imposed on the Potiguar basin during its history. These tectonic episodes were oriented with a $\sigma_{H,max}$ of NE-SW and NW-SE in the West of the basin and E-W and N-S in the East of the basin. Two scenarios were possible for this variation; in one scenario, stress fields with a different orientation were present in the West and East parts of the basin. The second scenario consisted of a regional stress field that locally changed orientation based on the geomechanical differences of the basement and sediment infill.

With the constructed basin model, the orientation of the horizontal principal stresses could be determined. figure 5.10a, 5.10b, 5.12a and 5.12b depict the orientation of the horizontal principal stresses at a depth of 2000 meters between the boundary of the basement and the sedimentary formations. The geology at this depth and stress fields have been implemented for figures 5.17a, 5.17b, 5.18a, 5.18b. Minor rotations of the principal stresses is present at every scenario, but the scenarios with 10 MPa show the largest change in orientation. At the 20 MPa compression, the horizontal stresses have a larger influence on the orientation and rotation is less prevalent. In scenario 4, the geomechanical property differences between the sedimentary facies and the basement is increased (figure 5.19a and 5.19b). This does not appear to have a large effect on the reorientation. In the current basin model, fault presence and therefore movement along the fault is not implemented as well as the size of the basin model required the use of a coarse model. The lack of these features therefore results in a degree of uncertainty and larger reorientations could occur when these features are implemented. In this model, reorientation of the horizontal principal stresses occurs at the basement/sedimentary boundary, where the difference between the geomechanical properties is largest, and reorientates towards the boundary.

5.3.3. Vertical stress distribution

In the section regarding stylolite analysis, the distribution of vertical stress - and in lesser form also horizontal stress - was determined throughout the Potiguar basin. The stress distribution was taken from stylolite samples of mainly two outcrops on the Western section of the basin. The large similarity of the stress and burial results led to the assumption that the Jandaira formation subsided uniformly throughout the basin. With the basin model the principal stresses were calculated using the basin geometry and geomechanical properties

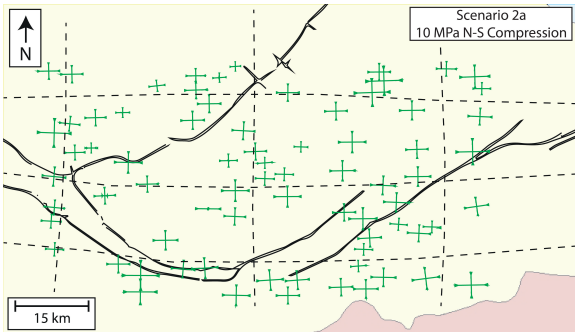

(a) Interpolation between the principal stress orientation results from scenario 2 with N-S compression.

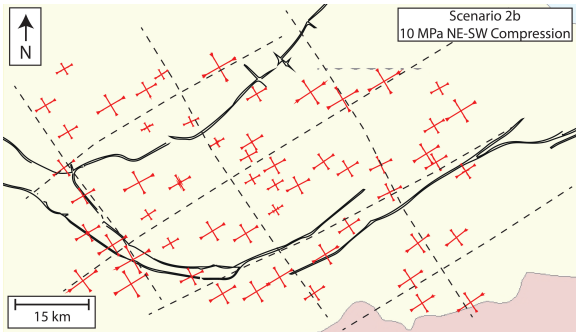

(b) Interpolation between the principal stress orientation results from scenario 2 with NE-SW compression.

Figure 5.17

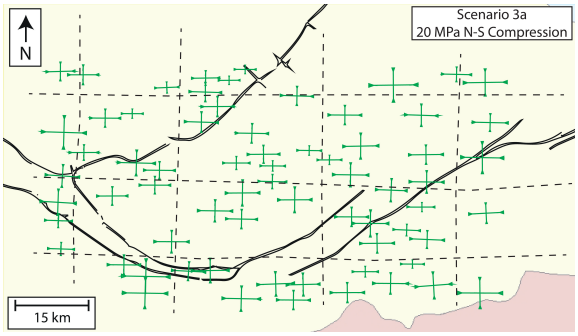

(a) Interpolation between the principal stress orientation results from scenario 3 with N-S compression.

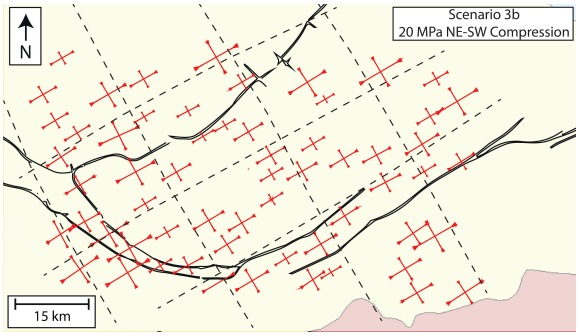

(b) Interpolation between the principal stress orientation results from scenario 3 with NE-SW compression.

Figure 5.18

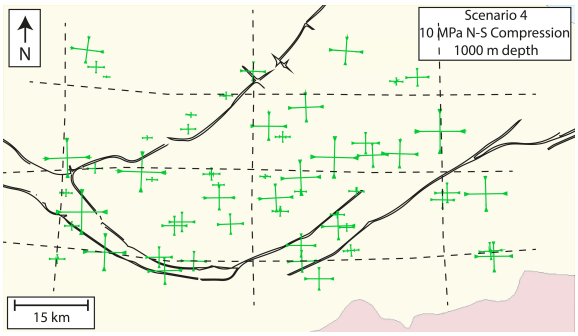

(a) Interpolation between the principal stress orientation results from scenario 4.

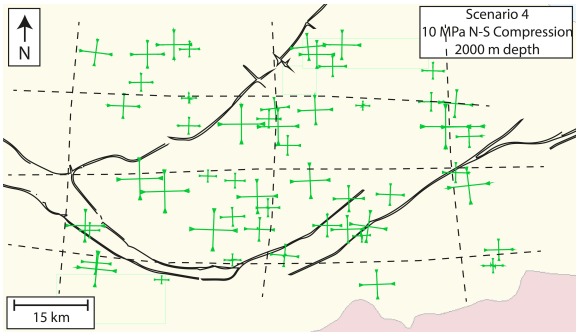

(b) Interpolation between the principal stress orientation results from scenario 4.

Figure 5.19

to also determine the stress distribution throughout the basin. The results from the vertical stress distributions were imaged on XY planes of 100 x 70 km and at a certain depth. Figures 5.20a, 5.20b and 5.20c show the vertical stress at a depth of 500, 750 and 1000 meters respectively. Although stress calculations at a shallow depth show significant noise, the figures show that the vertical stresses are in the same order of magnitude at the location of the two outcrops and the majority of the onshore Jandaira formation. These results show that uniform subsidence from the stylolite results, the geometry of the basin has little effect on the stress distribution at shallow depths and vertical stress exerted on the system produces similar stress magnitudes at the studied areas.

In the stylolite section, the effects of a horizontal compressional tectonic stress was also calculated. Results from these calculations lead to an average vertical stress of 15 MPa or 700 meters for 10 MPa horizontal

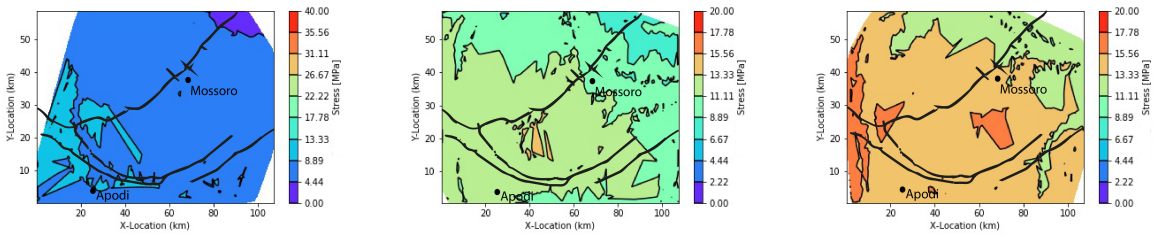

(a) σ_1 distribution on the XZ plane with uni-axial burial conditions at Z = 500 m.

(b) σ_1 distribution on the XZ plane with uni-axial burial conditions at Z = 750 m.

(c) σ_1 distribution on the XZ plane with uni-axial burial conditions at Z = 1000 m.

Figure 5.20: Distribution of σ_1 on the XZ plane with uni-axial burial conditions at varying depths.

stress and 20 MPa or 900 meters for 20 MPa horizontal stress. These scenarios are also modeled with the geomechanical model. Depicted in the pressure-depth plots of scenarios 1, 2 and 3 (figure 5.16a, 5.16b and 5.16c) are the vertical stress, maximum horizontal stress and minimum horizontal stress. From the modeling results, the vertical stress of scenario 2 is associated with a depth of 1000 meters and for scenario 3 a depth of 1500 meters. The geomechanical modeling results seem to be in accordance with the stylolite results. However, the distribution of $\sigma_{H,max}$ was not taken into account. For scenario 2, $\sigma_{H,max}$ is near equal to the the vertical stress and scenario 3 $\sigma_{H,max}$ is greater than the vertical stress. The equations used in the stylolite section to account for the tectonic stress assume that the vertical stress is still of greater magnitude to allow the formation of horizontal stylolites. The maximum horizontal stress is only used to determine the minimum horizontal stress through the Poisson ratio.

The figures show that for scenario 2, the vertical stress becomes σ_1 at a depth of around 1200 meters and for scenario 3 at a depth of 2500 meters. Until the formations are buried up to at least that depth, no horizontal stylolites are formed. In the stylolite section, the horizontal stylolite section showed burial depth results of 750 meters for 10 MPa horizontal tectonic stress and the vertical stylolite results indicated a horizontal stress of 13 MPa horizontal stress. The similar results from scenario 2 of the geomechanical model confirm the maximum burial depth of around 1000 ± 250 meters at a horizontal compression of 10 ± 5 MPa. For scenario 3, however, the results from the stylolite section show a depth of around 1500 meters are not represented with the geomechanical model, where σ_1 becomes vertically oriented at a depth of 2500 meters. A schematic representation is depicted in figure 5.21.

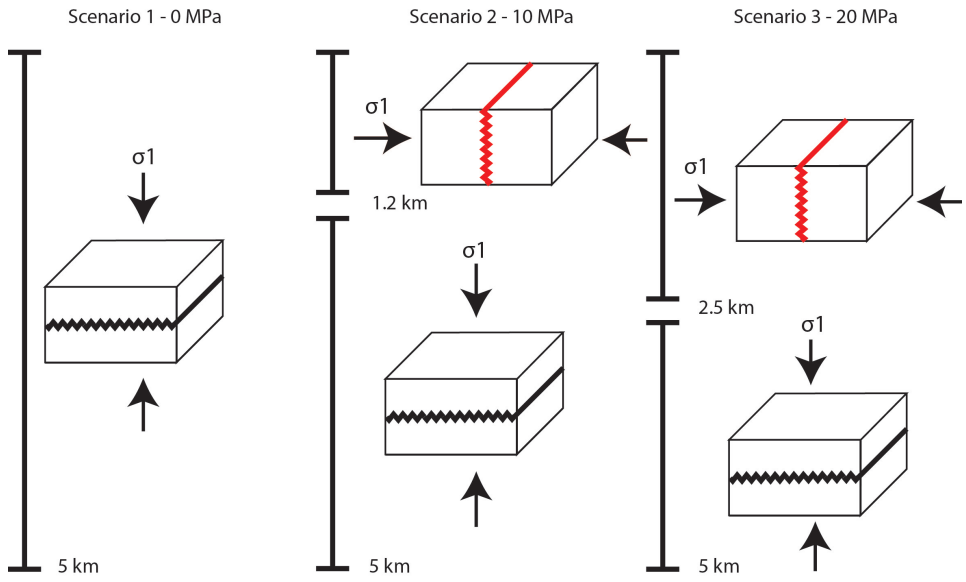

Figure 5.21: Schematic distribution of the depth of horizontal and vertical stylolite formation for scenarios 1, 2 and 3. Principal stress magnitudes were taken from the geomechanical modelling results.

5.3.4. Present day

The present day state of stress was implemented into the geomechanical model using horizontal stress ratios taken from Reis et al. (2013) (figure 5.22). The horizontal tectonic stress is lower than previous scenarios and with the coarse grid of the geomechanical model this results in more noise. However, due to the smaller horizontal stress the differences between the geomechanical properties of the basement and the sedimentary facies has a larger effect and more rotations occur towards the basement/sedimentary boundary. The rotations found in these results do not coincide with the large rotation in $\sigma_{H,max}$ orientation from E-W to N-S as is seen in the borehole breakouts of the wells surrounding the Potiguar basin.

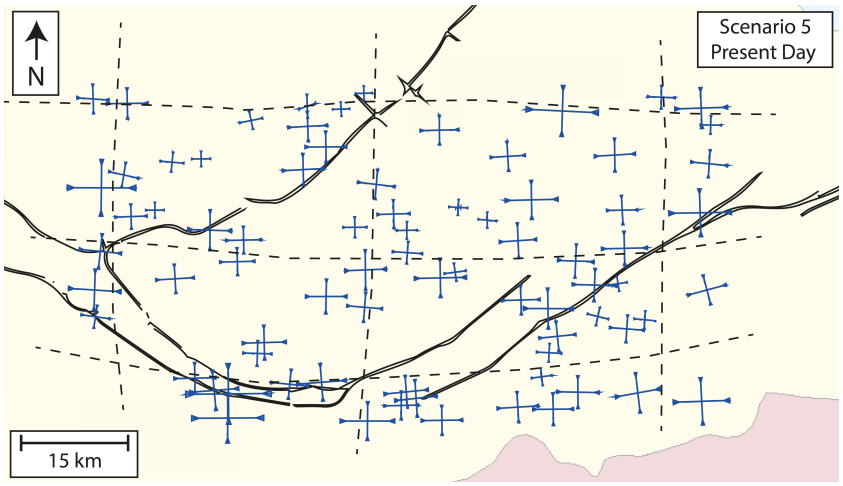

Figure 5.22: Interpolation between the principal stress orientation results from the present day state of stress scenario.

5.3.5. Further research

Further research on the geomechanical model of the Potiguar basin could be done in a number of ways such as implementing strain relations to determine principal stress rotations, creating a finer grid for more precise stress distributions, implementing fault offsets to determine the geomechanical processes around the large offset faults or to extend the model to the offshore section of the Potiguar basin. The 3D Grid of this study was cropped in a smaller area due to numerous interpolation anomalies that were generated. Better boundary conditions and erosional surfaces could allow for a larger grid and include the offshore section of the Potiguar basin.

The offshore section of the Potiguar is of interest to the O&G industry where multiple reservoirs are located. Though further from the main rifting structure onshore, the Neo-Proterozoic weak zones are present. Because the area is further from the basin structure, the regional uplift (associated with the present altitude of the onshore Jandaira formation) could be absent. With the fluid flow timeline proposed by Giovanni et al. (2017), an absence of the reactivation of basin tectonic results in an absence of the large fault systems of that is present on the onshore section of the Jandaira formation. Without these fracture systems, the permeability of the Jandaira formation is very low due to the poor porosity associated with diagenesis effects of groundwater fluid flow in the early stages after deposition. However, if the open fault systems are present in the offshore section, the basin model can be extended to determine the stress magnitudes present and predictions of fault density/length can be made by comparison with the outcropping Jandaira formation.

6

Conclusions

This study focussed on the distribution of the state of stress in the Potiguar basin through a multi-scale approach. In the small scale, outcrop studies and stylolite sample analysis have been conducted. In the large scale, a geomechanical model is constructed of the Potiguar basin and subjected to tectonic scenarios. The orientation of the horizontal principal stresses of the two compressional episodes were studied through outcrop studies and a geomechanical model of the basin. Outcrop studies resulted in a difference in horizontal principal stress orientation from the west to east of the basin of approximately 30 degrees and a difference in principal stress orientation in the main rift area. Results from geomechanical modelling show that rotation of the horizontal stresses occurs due to the difference in geomechanical properties of the basement and sedimentary facies. However, the rotation of the horizontal stresses is of a lesser degree than the differences found in the field. Local reorientation occurred in the areas close to the basement/sedimentary boundary where regional horizontal compression reoriented locally towards the boundary.

The maximum burial depth to which the carbonate Jandaira formation was subject to was calculated through stylolite analysis of samples in the Western part of the Jandaira formation in the Potiguar basin. Fourier analysis of the stylolite traces allowed for the determining the maximum stress values that were present during stylolite formation. These stress values were used to calculate the maximum burial depth of the formation under uni-axial conditions and scenarios of 10 MPa and 20 MPa horizontal tectonic stress. The results from the stylolite analysis on the horizontal stylolites showed an average vertical stress of 13 MPa, which is associated with an average burial depth of 500 meters. Horizontal tectonic stress scenarios of 10 MPa and 20 MPa led to an average burial depth of 700 and 900 meters, respectively. The variations between the outcrops decrease proportional to an increase of tectonic stress to between 150 (to 200 – taken from one sample) meters burial depth at a tectonic influence of 20 MPa. Implementing the results from previous studies (Bertotti et al., 2017) show small regional variations in the order of 20 % and indicate similar amounts of subsidence occurred between both regions.

A geomechanical basin model was constructed of the Potiguar basin and extends 100 x 70 x 5 km in the main rifting area. Horizontal tectonic compression of 10 and 20 MPa was exerted on the geomechanical model and the distribution of the principal stress orientation and magnitudes were compared with the previous sections. The resulting σ_1 were determined and showed a slight increase in burial depth for all similar scenarios of tectonic stress. However, the scenario of 20 MPa horizontal compression showed that the vertical stress required to create the horizontal stylolites is σ_2 up to a depth of around 2500 meters, when it becomes σ_1. For the scenario of 10 MPa horizontal compression, the depth at which the vertical stress becomes σ_1 is around 1500 meters. Aside of the vertical stress difference that was observed of around 30%, the burial depth at for this scenario is around 1000 meters.

Results from the stylolite analysis show a burial depth of 700 meters with 10 MPa horizontal compression and the vertical stylolite result indicate horizontal compression of 13 MPa. In this case, the results from the small scale horizontal and vertical stylolite analysis are similar to the results of the geomechanical model and indicate a regional burial depth of 1000 ± 250 meters under 10 ± 5 MPa horizontal compression.

7

Acknowledgements

Firstly, I would like to thank Prof. Dr. G.Bertotti for providing guidance before, during and after field work in Brazil. I would also like to thank Petrobras for providing financial support of the field work. I would like to thank the geology department of the Federal University of Rio Grande do North in Brazil and in particular Prof. H. Bezerra and the PhD candidates Christiane Menezes and Juliana Rabelo for accompanying me throughout the field work and helping in any way they could. I would also like to thank Kevin Bisdom and Quinten Boersma for aiding in my work and furthering the discussions. Finally, I would also like to thank Alanny Christiny Costa de Melo for providing basin data such as geological maps, fault dimensions, gravity anomaly maps and seismic.

8

List of Symbols

σ_1	Maximum Prinicpal Stress (MPa)
σ_3	Minimum Principal Stress (MPa)
σ_2	Intermediate Principal Stress (MPa)
γ	Surface Tension (N/m)
E	Young's Modulus (MPa)
L_c	Crossover Length (mm^{-1})
σ_x	Horizontal Stress in the x-Direction (MPa)
σ_y	Horizontal Stress in the y-Direction (MPa)
ν	Poisson's Ratio
S_{tect}	Tectonic Stress (MPa)
$\sigma_{H,max}$	Maximum Horizontal Stress (MPa)
$\sigma_{H,min}$	Minimum Horizontal Stress (MPa)
σ_v	Vertical Stress (MPa)
ρ	Density ($kg/m3^3$)
g	Gravitational Constant ($m^3kg^{-1}s^{-2}$)
z	Depth (m)

Bibliography

[1] Araripe, P.T. & Feijo, F.J. (1994) *Bacia Potiguar*. Boletim degeociencias da petrobras, 8, pp. 127-141.

[2] Barabási, A.L., Stanley & E.H., Matos, R.M.D. (1995) *Fractal Concepts in Surface Growth*. Cambridge Univ. Press, New York.

[3] Bertani, R.T., Neto & A.F., Matos, R.M.D. (1987) *O Habitat Do Petroleo e as perspectivas exploratorias da bacia potiguar emersa*. Boletim degeociencias da petrobras, 1, pp. 41-49.

[4] Bertani, R.T., de Costa, I.G., Matos & R.M. (1990) *Evolacao tectono-sedimentar, estilo estrutural, e habitat do petroleona bacia Potiguar*. Origem e Evolucao de Bacias Sedimentares, Petrobras (Ed. by G.P. Raja Gabagli & E.G. Milani), pp. 291–310.

[5] Bertotti, G., de Graaf, S., Bisdom, K., Oskam, B., Vonhof, H.B., Bezerra, F.H.R., Reijmer, J.J.G. Cazarin, L. (2017) *Fracturing and fluid-flowduring post-rift subsidence in carbonates of the Jandaira Formation, Potiguar Basin, NE Brazil*. Basin Research, pp. 1-18.

[6] Ebner, M., Koehn, D., Toussaint, R., Renard, F., & Schmittbuhl, J. (2009) *Stress sensitivity of stylolite morphology*. Earth and Planetary Science Letters, 277(3), pp. 394-398.

[7] van Eijk, M.M. (2014) *Analysis of the fracture network in carbonate rocks of the Jandaíra Formation in northeast Brazil*. Unpublished MSc Thesis VU University Amsterdam.

[8] Gercek, H. (2006) *Poisson's ratio values for rocks*. International Journal of Rock Mechanics & Mining Sciences, 44(2007), pp. 1-13.

[9] de Graaf, S. (2015) *Development of the vein network in the Jandaira formation, northeast Brazil*. Unpublished MSc Thesis VU University Amsterdam.

[10] Gurgel, S. P. P., Bezerra, F. H. R., Correa, A. C. B., Marques, F. O., Maia, R. P. (2013) *Cenozoic uplift and erosion of structural landforms in NE Brazil*. Journal of Geophysical Research, 103, pp. 27091-27105

[11] Hameka, F. (2015) *Generations and infill of the veins in the Jandaira Formation near Apodi, Rio Norte, Brazil*. Unpublished MSc Thesis VU University Amsterdam.

[12] Kirkpatrick, J. D., Bezerra, F. H. R., Shipton, Z. K., Do Nascimento, A. F., Pytharouli, S. I., Lunn, R. J., & Soden, A. M. (2013). *Scale-dependent influence of pre-existing basement shear zones on rift faulting: a case study from NE Brazil*. Journal of the Geological Society, 170(2), pp. 237-247.

[13] Koehn, D., Ebner, M., Renard, F., Toussaint, R., & Passchier, C. W. (2012). *Modelling of stylolite geometries and stress scaling*. Earth and Planetary Science Letters, 341, pp. 104-113.

[14] Lima, C., Nascimento, E. & Assumpcao, M. (97). *Stress orientations in Brazilian sedimentary basins from breakout analysis: implications for force models in the South American plate*. Journal of Geophysics, 130, pp. 112-124.

[15] de Matos, R.M.D. (1992). *The Northeast Brazilian Rift System*. Tectonics, 11(4) pp. 766.

[16] de Matos, R.M.D. (2000). *Tectonic evolution of the equatorial South Atlantic.*. AGU Geophysical Monograph, 115, pp. 331-354.

[17] Meakin, P. (1998). *Fractals: Scaling and Growth Far From Equilibrium*. Cambridge Univ. Press, New York.

[18] Costa de Melo, A.C., de Castro, D.L., Bezerra, R.F.H. & Bertotti, G. (2016). *Rift fault geometry and evolution in the Cretaceous Potiguar Basin (NE Brazil) based on fault growth models.*. Boletim Geociencias Petrobras, 71, pp. 96-107.

[19] Oskam, B. (2015) *Stylolite roughness as indicator of the vertical stress conditions in the Potiguar basin, Northeast Brazil*. Unpublished MSc Thesis VU University Amsterdam.

[20] Pessoa Neto, O.C., Soares, U.M., da Silva, J.G.F., Roesner, E.H., Florencio, C.P. & de Souza, C.A.V. (2007). *Bacia Potiguar*. Boletim Geociencias Petrobras, 15(2), pp. 357-369.

[21] Schaller, H. & Sampaio, A.V. (1968). *Introducao a estratigrafia da Bacia Potiguar*. Boletim Geociencias Petrobras, pp. 24.

[22] Renard, F., Schmittbuhl, J., Gratier, J. P., Meakin, P., & Merino, E. (2004) *Roughness of stylolites: implications of 3D high resolution topography measurements*. Phys. Rev. Lett., 93(23), 238501.

[23] Renard, A., Schultz (1993) *Brittle strength of basaltic rock masses with applications to Venus*. Journal of Geophysical Research, 98, 10883-10895.